The calcium-binding protein ALG-2 regulates protein secretion and trafficking via interactions with MISSL and MAP1B proteins

Received for publication, June 2, 2017, and in revised form, August 31, 2017 Published, Papers in Press, September 1, 2017, DOI 10.1074/jbc.M117.800201

Terunao Takahara[‡1], **Kuniko Inoue**[‡], **Yumika Arai**[‡], **Keiko Kuwata**[§], **Hideki Shibata**[‡], **and Masatoshi Maki**[‡2]

From the [‡]*Department of Applied Molecular Biosciences, Graduate School of Bioagricultural Sciences, and the* [§]*Institute of Transformative Bio-Molecules (WPI-ITbM), Nagoya University, Furo-cho, Chikusa-ku, Nagoya, Aichi 464-8601, Japan*

Edited by Roger J. Colbran

Mobilization of intracellular calcium is essential for a wide range of cellular processes, including signal transduction, apoptosis, and vesicular trafficking. Several lines of evidence have suggested that apoptosis-linked gene 2 (ALG-2, also known as *PDCD6*), a calcium-binding protein, acts as a calcium sensor linking calcium levels with efficient vesicular trafficking, especially at the endoplasmic reticulum (ER)-to-Golgi transport step. However, how ALG-2 regulates these processes remains largely unclear. Here, we report that MAPK1-interacting and spindle-stabilizing (MISS)-like (MISSL), a previously uncharacterized protein, interacts with ALG-2 in a calcium-dependent manner. Live-cell imaging revealed that upon a rise in intracellular calcium levels, GFP-tagged MISSL (GFP-MISSL) dynamically relocalizes in a punctate pattern and colocalizes with ALG-2. MISSL knockdown caused disorganization of the components of the ER exit site, the ER-Golgi intermediate compartment, and Golgi. Importantly, knockdown of either MISSL or ALG-2 attenuated the secretion of secreted alkaline phosphatase (SEAP), a model secreted cargo protein, with similar reductions in secretion by single- and double-protein knockdowns, suggesting that MISSL and ALG-2 act in the same pathway to regulate the secretion process. Furthermore, ALG-2 or MISSL knockdown delayed ER-to-Golgi transport of procollagen type I. We also found that ALG-2 and MISSL interact with microtubule-associated protein 1B (MAP1B) and that MAP1B knockdown reverts the reduced secretion of SEAP caused by MISSL or ALG-2 depletion. These results suggest that a change in the intracellular calcium level plays a role in regulation of the secretory pathway via interaction of ALG-2 with MISSL and MAP1B.

Mobilization of intracellular calcium is essential for a wide range of cellular processes, including signal transduction, apoptosis, and vesicular trafficking (1, 2). In the secretory pathway, nascent secretory proteins enter into the endoplasmic reticulum (ER),[3] and transport vesicles containing the secretory proteins bud from specialized ER membranes designated as the ER exit site (ERES) or transitional ER by virtue of the coat protein complex II (COPII) machinery and then move to Golgi via the ER-Golgi intermediate compartment (ERGIC) (3, 4). Golgi-derived transport vesicles are ultimately fused with plasma membranes to release the secretory proteins. Recent studies have indicated that calcium released from the ER and transport vesicles appears to play an important role in the regulation of proper secretion. Indeed, the previous study using BAPTA-AM (1,2-bis(2-aminophenoxy)ethane-*N*,*N*,*N*′,*N*′-tetraacetic acid acetoxymethyl ester), a cell-permeable calcium chelator, indicated that a local calcium signal is required for ERGIC-to-Golgi trafficking in ER-to-Golgi transport (5, 6). In addition, reduction of the calcium level in the ER or transport vesicles by treatment of cells with cyclopiazonic acid, a reversible sarco/endoplasmic reticulum Ca^{2+}-ATPase (SERCA) inhibitor, resulted in a decrease in the rate of ER-to-Golgi transport (7), although the detailed mechanism of calcium requirement remains largely unclear.

Apoptosis-linked gene 2 (ALG-2, also known as *PDCD6*) is a calcium-binding protein that possesses the domain of five EF-hands (penta-EF-hand (PEF) domain) (8). Binding of calcium to ALG-2 induces a conformational change (9), which facilitates the interaction with various proteins, including ALG-2-interacting protein X (ALIX) (an auxiliary protein of the endosomal sorting complex required for transport (ESCRT)) (10, 11), Sec31A (outer shell component of COPII) (12–14), and annexin A11 (a calcium-dependent lipid-binding protein) (15, 16). Through sequence comparison among regions of ALIX, Sec31A, and PLSCR3 responsible for binding with ALG-2, we previously identified two different types of binding motif of

This work was supported in part by Grant-in-aid for Young Scientists (B) 15K18680 and Grant-in-aid for Scientific Research (C) 17K07752 (to T. T.), Grant-in-aid for Scientific Research (B) 26292050 and 17H03803 (to M. M.), Grant-in-aid for Scientific Research (C) 15K07384 (to H. S.), and Grant-in-aid for Scientific Research on Innovative Areas JP15H05955 (to K. K.). The authors declare that they have no conflicts of interest with the contents of this article.

This article contains supplemental Figs. S1–S4 and Movies S1–S2.

[1] To whom correspondence may be addressed. Tel.: 81-52-789-4183; Fax: 81-52-789-5542; E-mail: takahara@agr.nagoya-u.ac.jp.

[2] To whom correspondence may be addressed. Tel.: 81-52-789-4088; Fax: 81-52-789-5542; E-mail: mmaki@agr.nagoya-u.ac.jp.

[3] The abbreviations used are: ER, endoplasmic reticulum; MISS, MAPK1-interacting and spindle-stabilizing; MISSL, MAPK1-interacting and spindle-stabilizing-like; SEAP, secreted alkaline phosphatase; ERES, ER exit site; COPII, coat protein complex II; ERGIC, ER-Golgi intermediate compartment; SERCA, sarco/endoplasmic reticulum Ca^{2+}-ATPase; PEF, penta-EF-hand; ALIX, ALG-2-interacting protein X; ESCRT, endosomal sorting complex required for transport; ABM, ALG-2-binding motif; TFG, Trk-fused gene; VSV-G, vesicular stomatitis virus glycoprotein; TG, thapsigargin; BFA, brefeldin A; HBSS, Hanks' balanced salt solution; siRNA, small interfering RNA; IP, immunoprecipitation; KO, knockout; UTR, untranslated region; ANOVA, analysis of variance; PFA, paraformaldehyde; EGFP, enhanced GFP.

ALG-2, and we designated the motifs as ALG-2-binding motif (ABM)-1 and ABM-2 (17). The two motifs were further characterized by X-ray crystal structure analysis of ALG-2 together with the binding peptide derived from ALIX or Sec31A and by mutagenesis analysis of the minimal binding motif (9, 18), and it was shown that ABM-1 is composed of PPYP$(X)_4$YP, whereas ABM-2 is (PΦ)PX(PΦ)G(FW)Ω (where PΦ is Pro or hydrophobic; FW is Phe or Trp; Ω is large side chain; and X, variable) (19). ALG-2 forms a homodimer (10, 20, 21) and a heterodimer with another PEF-containing protein, peflin (21). The ALG-2 homodimer is able to bind to two different proteins simultaneously and thereby can function as an adaptor to regulate calcium-dependent cellular processes. For instance, ALG-2 binds to both ALIX and TSG101, an ESCRT-I protein (22, 23), or binds to both Sec31A and annexin A11 to regulate ER-to-Golgi transport (16). ALG-2 also binds to Trk-fused gene (TFG) molecules to promote TFG polymerization by its adaptor function (24).

Several recent studies have suggested that ALG-2 regulates the secretory pathway at the ER-to-Golgi transport step. In *in vitro* experiments, ALG-2 was shown to inhibit homotypic fusion of COPII vesicles (25) and COPII vesicle budding from the ER membrane (26), although the effects of ALG-2 on the fusion and budding remain to be established *in vivo*. More recent studies have suggested that ALG-2 may regulate ER-to-Golgi transport at least in the specific cellular context *in vivo* (7, 16, 27). Knockdown of ALG-2 or its binding partner annexin A11 enhanced the rate of ER-to-Golgi transport of a temperature-sensitive mutant of vesicular stomatitis virus glycoprotein (VSV-G) in HT1080 cells (16), whereas no difference in the rate of transport was observed in HeLa cells (12). In contrast, Helm *et al.* (7) reported that ALG-2 knockdown or ALG-2 overexpression together with a fragment containing the ALG-2-binding region of Sec31A can delay ER-to-Golgi transport. In addition, knockdown of peflin, potentially leading to an increase in the population of ALG-2 homodimers, promotes ER-to-Golgi transport (27). Thus, ALG-2 may be an important calcium sensor linking intracellular and/or luminal calcium levels with regulatory machinery of the secretory pathway. Indeed, it was reported recently that the ALG-2–peflin heterodimer acts as a coadaptor relaying a transient calcium rise into CUL3-mediated Sec31A ubiquitylation, allowing the formation of large COPII vesicles responsible for collagen secretion (28), although the regulatory mechanism(s) of ALG-2 for general ER-to-Golgi transport in response to an alteration of the calcium level remains largely unknown.

We previously searched for novel ALG-2-interacting proteins through *in silico* screening based on the presence of ALG-2-binding motifs within proline-rich regions, and we found several new candidate proteins by far-Western analysis (29). One of the candidates is MAPK1-interacting and spindle-stabilizing (MISS)-like (MISSL). Although the primary sequence of MISSL is similar to that of MISS (30), the functional regions of MISS, including a MAPK-docking site, a PEST sequence, and a bipartite nuclear localization signal, are lacking in MISSL, and the cellular function of MISSL has therefore remained completely unknown. In this study, we found that MISSL indeed interacts with ALG-2 in a calcium-dependent manner and that MISSL and ALG-2 act in the same pathway regulating the secretion process. Furthermore, our results suggest that ALG-2 links MISSL and microtubule-associated protein 1B (MAP1B) in a calcium-dependent manner, which likely plays an important role in the regulation of efficient secretion.

Results

MISSL binds to ALG-2 in a calcium-dependent manner

We previously identified several potential ALG-2-binding proteins through *in silico* screening and far-Western blotting using biotin-labeled ALG-2 as a probe (29). Here, we focused on MISSL, a previously uncharacterized protein, and examined further whether MISSL indeed binds to ALG-2. To examine the interaction between MISSL and ALG-2, GFP-tagged MISSL (GFP-MISSL) was transiently expressed in HeLa cells and was tested for interaction with endogenous ALG-2 (Fig. 1*A*). Endogenous ALG-2 was coimmunoprecipitated with GFP-MISSL but not with GFP, and the interaction was diminished in the presence of EGTA, a calcium chelator. To determine whether endogenous MISSL interacts with endogenous ALG-2 as well, endogenous MISSL was immunoprecipitated using an anti-MISSL antibody. As shown in Fig. 1*B*, ALG-2 was coimmunoprecipitated with MISSL in the presence of calcium but not EGTA. Together, these results suggest that MISSL is a *bona fide* ALG-2-interacting partner.

Our previous results indicated that ALG-2 preferentially binds to two different types of motifs (ABM-1 and ABM-2) present in proline-rich regions (9, 17, 18). MISSL contains two ABM-1-like sequences as shown in Fig. 1*C*. To determine whether the two sites are essential for binding with ALG-2, we compared the interactions of GFP-MISSL and a mutant (GFP-MISSLΔΔ) lacking the two sequences (101–117 and 167–175 amino acids) with ALG-2. GFP-MISSL and GFP-MISSLΔΔ showed similar interactions with ALG-2 by immunoprecipitation analysis (Fig. 1*D*), suggesting that MISSL is still able to bind to ALG-2 through a region different from the two sequences. To narrow down the ALG-2-binding site(s) in MISSL, GFP-MISSL, and its N- or C-terminal deletion mutants were transiently expressed, and their binding abilities were tested by far-Western blotting using biotin-labeled ALG-2 as a probe (Fig. 1*E*). Deletion of either the N-terminal (Δ1–138) or C-terminal region (Δ93–245 and Δ147–245) dramatically reduced the binding of ALG-2. Similarly, endogenous ALG-2 was efficiently coimmunoprecipitated with the full-length and Δ1–90 mutant but to a lesser extent with Δ1–138, Δ93–245, and Δ147–245 mutants (Fig. 1*F*). Thus, MISSL appears to bind to ALG-2 through multiple sites in the whole region, attributed to high proline-rich contents in MISSL. The involvement of multiple sites in the interaction with ALG-2 is also found in proteins containing ABM-1-like, such as TSG101, VPS37B, and VPS37C, and it has been difficult to identify particular sites sufficient for binding to ALG-2 in those proteins (data not shown). We also cannot rule out the possibility that the deletion of the N- or C-terminal portion of MISSL (*e.g.* Δ1–138 or Δ147–245) perturbs the tertiary structure or conformation of the remaining region, thereby leading to the reduced binding to ALG-2.

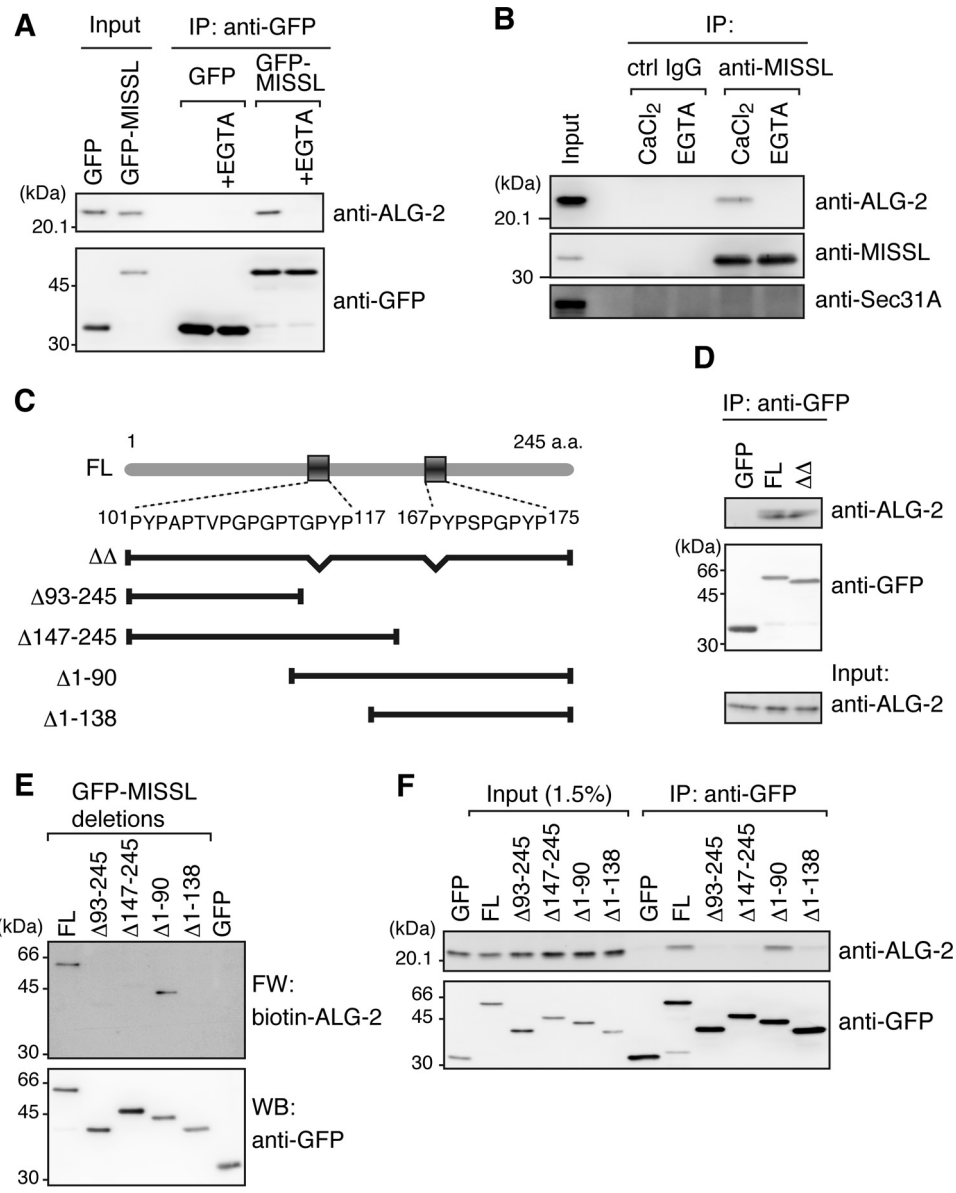

Figure 1. MISSL is a *bona fide* ALG-2-interacting protein. *A,* HeLa cells were transiently transfected with plasmids for expression of GFP or GFP-MISSL, and cell lysates were subjected to immunoprecipitation (*IP*) with an anti-GFP antibody in the absence or presence of 5 mM EGTA (+*EGTA*). The immunocomplexes were analyzed by immunoblotting with the indicated antibodies. *B,* HeLa cell lysate was subjected to IP with an anti-MISSL antibody (sc-243408) or control (*ctrl*) IgG in the presence of 5 mM EGTA or 100 μM $CaCl_2$. The immunocomplexes were analyzed by immunoblotting with the indicated antibodies. *C,* schematic representation of MISSL structure. Two putative ABM-1-like sequences, which are located at 101–117 and 167–175 amino acids (*a.a.*), are shown. The deletion mutants used are also shown below the MISSL structure. *D,* HeLa cells were transiently transfected with GFP and GFP-tagged full-length MISSL (*FL*) GFP-MISSL lacking both 101–117 and 167–175 amino acids (ΔΔ), and the cell lysates were subjected to IP with the anti-GFP antibody. The immunocomplexes were analyzed by immunoblotting with the indicated antibodies. *E,* HEK293T cells transfected with the plasmids for expression of the indicated proteins were lysed, and GFP or GFP-MISSL variants were immunopurified using the anti-GFP antibody. The immunoprecipitates were separated by SDS-PAGE and subjected to far-Western (*FW*) analysis using biotin-labeled ALG-2 (*biotin-ALG-2*) and to Western blotting (*WB*) with the anti-GFP antibody. *F,* IP analyses using HeLa cells transiently expressing GFP, GFP-MISSL full-length (*FL*), or GFP-MISSL deletions were performed as in *D*.

MISSL dynamically relocates at ALG-2-positive dots upon intracellular calcium rise

To investigate the subcellular localization of MISSL in living cells, GFP-MISSL was transiently expressed in HeLa cells, and the localization was observed through live cell imaging. We also expressed a fluorescent calcium indicator, R-GECO1 (31), to monitor the intracellular calcium rise simultaneously. To increase intracellular calcium by a physiological condition, we used amino acid addition to amino acid-starved cells, a known treatment to increase intracellular calcium (32). Under the amino acid-starved condition, GFP-MISSL was diffusely distributed throughout the cells (Fig. 2*A*, −*AA*). Upon amino acid addition, intracellular calcium was increased as shown by the enhanced fluorescence signal of R-GECO1 (Fig. 2, *A* and *B*), and GFP-MISSL rapidly relocalized to the punctate pattern (Fig. 2*A*, +*AA*, and supplemental movie S1). Similar relocalization of GFP-MISSL was also observed when thapsigargin (TG), a SERCA inhibitor, was used to artificially increase the cytosolic calcium level (Fig. 2*C*, $t = 83$ s). Furthermore, the appearance of the GFP-MISSL puncta was transient and correlated with the

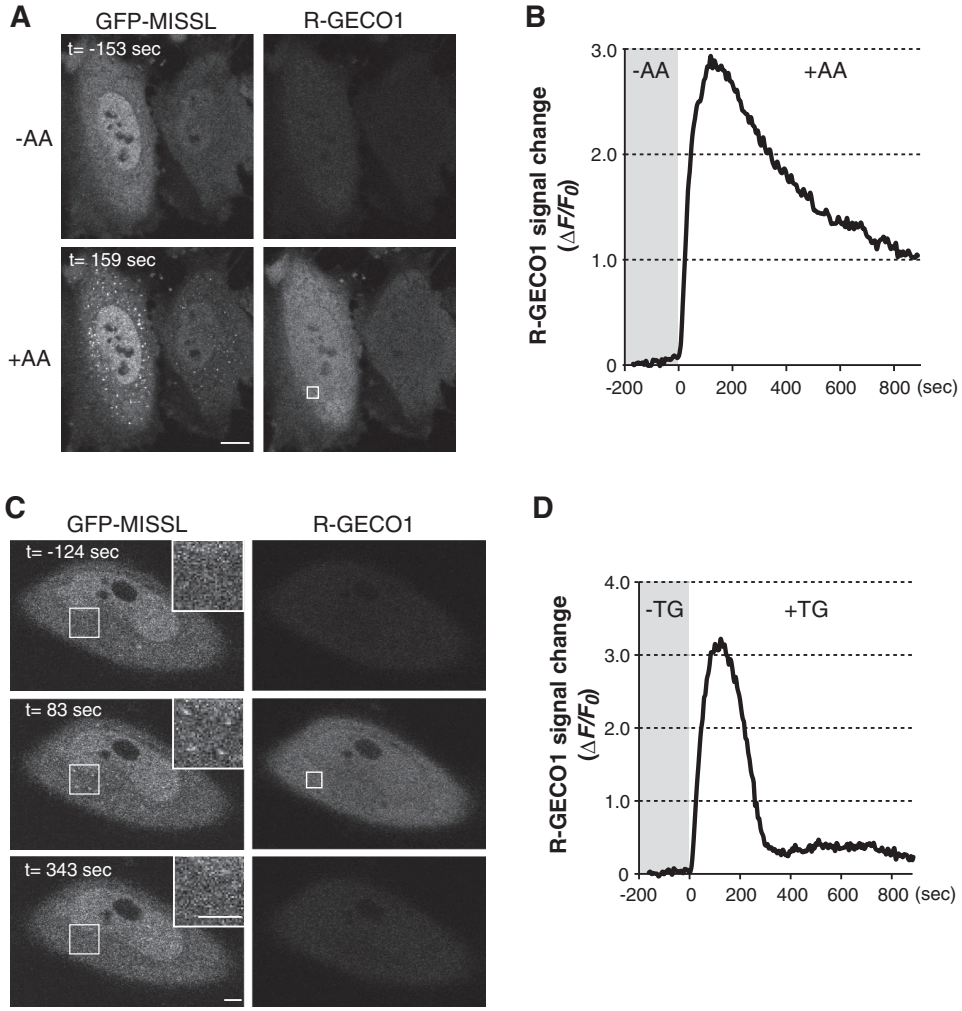

Figure 2. MISSL relocalizes to ALG-2-positive compartments upon a calcium rise in living cells. *A,* HeLa cells transiently expressing both GFP-MISSL and R-GECO1 were starved of amino acids for 60 min, and then an amino acid mixture was added ($t = 0$). Time-lapse images were captured before (*−AA*) and after (*+AA*) amino acid supplementation. Representative images of GFP-MISSL and R-GECO1 before (*−AA*, $t = -153$ *s*) and after (*+AA*, $t = 159$ *s*) are shown. *Bar,* 10 μm. *B,* changes of R-GECO1 fluorescent intensities in the area indicated by a *rectangle* in the R-GECO1 image in *A* are plotted. *C,* HeLa cells transiently expressing both GFP-MISSL and R-GECO1 were treated with thapsigargin (*TG*) at $t = 0$. Time-lapse images before and after TG treatment were captured. Representative images of GFP-MISSL and R-GECO1 before ($t = -124$ *s*) and after ($t = 83$ *s* and $t = 343$ *s*) are shown. *Insets* show magnified images of the region indicated by *white squares*. *Bars,* 5 μm. *D,* changes of R-GECO1 fluorescent intensities in the area indicated by a *rectangle* in the R-GECO1 image in *C* are plotted.

intracellular calcium rise, because GFP-MISSL puncta disappeared at the time when the intracellular calcium level returned to the original level, which was monitored by R-GECO1 fluorescent signal changes (Fig. 2, *C* and *D*, and supplemental movie S2).

To determine whether ALG-2 is involved in the GFP-MISSL relocalization, we first examined whether the GFP-MISSL puncta colocalized with ALG-2. To this end, both GFP-MISSL and mCherry-tagged ALG-2 (mCh-ALG2) were transiently expressed in HeLa cells. Under the amino acid-starved condition, most of the GFP-MISSL and mCh-ALG-2 were diffuse throughout the cells, but a small population of GFP-MISSL tended to form small puncta that overlapped with mCh-ALG-2 puncta (Fig. 3*A*, *−AA, inset*). Upon intracellular calcium rise caused by amino acid replenishment, mCh-ALG-2 also dynamically changed its location and formed large puncta (Fig. 3*A*, *+AA*). Consistent with MISSL binding to ALG-2 (Fig. 1, *A* and *B*), GFP-MISSL puncta were overlapped with mCh-ALG-2 puncta upon calcium rise (Fig. 3*A*, *+AA, Merge* and *graph*). To further examine whether the GFP-MISSL relocalization relies on ALG-2, the cellular ALG-2 level was reduced by an RNA interference method (Fig. 3, *B* and *C*). Depletion of ALG-2 significantly reduced GFP-MISSL puncta formation, although the degrees of calcium rise after amino acid supplementation were similar in both cell types (Fig. 3*B*). Furthermore, GFP-MISSLΔ147–245, which failed to bind to ALG-2 (Fig. 1), did not relocalize to ALG-2-positive dots upon amino acid replenishment (Fig. 3*D*). These results suggest that ALG-2 recruits MISSL to the sites where ALG-2 functions upon calcium rise.

ALG-2 is known to bind several proteins (19, 29, 33). Of the known interacting proteins, Sec31A was shown to be the strong binding partner of ALG-2, and most of ALG-2 colocalized with Sec31A-positive dots (12–14). Sec31A is a component of the outer coat of the COPII vesicle and is used for an ERES marker. To investigate the subcellular localization of MISSL, we immunostained MISSL and ALG-2 together with several organelle markers, including Sec31A. Unfortunately, none of the three commercially available antibodies against endogenous MISSL

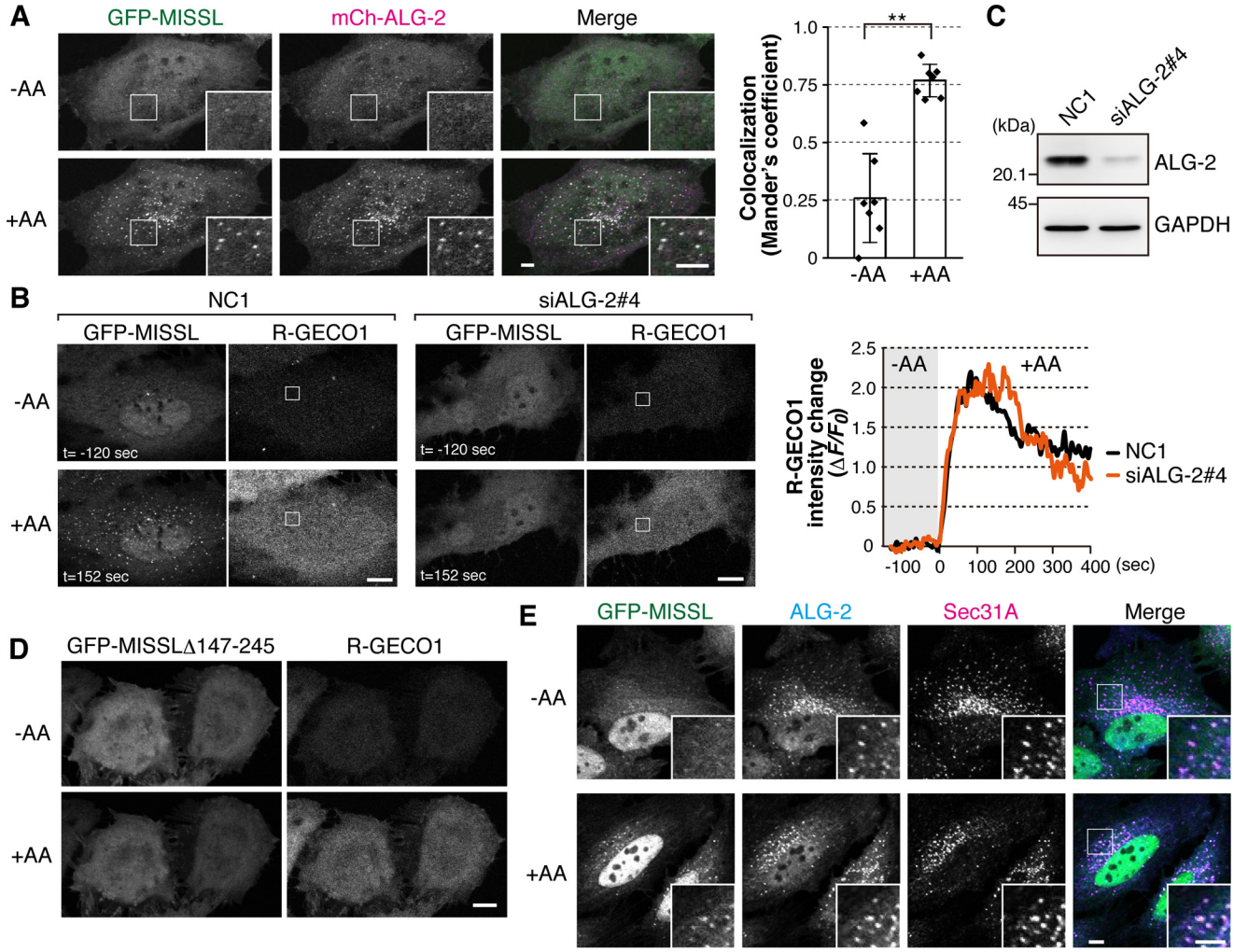

Figure 3. MISSL is recruited to and colocalizes with ALG-2 at the ERES. *A,* GFP-MISSL puncta colocalize with mCh-ALG-2 puncta upon a calcium rise. HeLa cells transiently expressing both GFP-MISSL and mCherry-ALG-2 (*mCh-ALG-2*) were starved of amino acids for 50 min, and then an amino acid mixture was added. Representative time-lapse images of GFP-MISSL and mCh-ALG-2 before (−*AA*) and after (+*AA*) addition of the amino acid mixture are shown. *Bars,* 5 μm. Mander's correlation coefficient between GFP-MISSL and mCh-ALG-2 before (−*AA*) and after (+*AA*) addition of amino acid mixture was graphed as mean ± S.D. ($n = 7$). **, $p < 0.01$, two-tailed *t* test. *B,* knockdown of ALG-2 resulted in failure of the formation of GFP-MISSL puncta upon a calcium rise. HeLa cells that had been transfected with siRNA for a control (*NC1*) or ALG-2 (*siALG-2#4*) were transiently transfected with plasmids expressing GFP-MISSL and R-GECO1. The cells were starved of amino acids for 50 min, and then an amino acid mixture was added at $t = 0$. Time-lapse images of GFP-MISSL and R-GECO1 before (−*AA*, $t = -120$ *s*) and after (+*AA*, $t = 152$ *s*) are shown. Changes of fluorescent intensities of R-GECO1 at the region shown in the R-GECO1 images during the experiment are plotted. *Bars,* 10 μm. *C,* HeLa cells were transfected with siRNA for a control (*NC1*) and ALG-2 (*siALG-2#4*), and the cell lysates were analyzed by immunoblotting with the indicated antibodies. *D,* HeLa cells transiently expressing both GFP-MISSLΔ147–245 and R-GECO1 were starved of amino acids for 50 min, and then an amino acid mixture was added. Representative images of GFP-MISSLΔ147–245 and R-GECO1 before (−*AA*) and after (+*AA*) addition of the amino acid mixture are shown. *Bar,* 10 μm. *E,* GFP-MISSL puncta colocalize with Sec31A and ALG-2. HeLa cells transiently expressing GFP-MISSL were starved of amino acids for 50 min (−*AA*), and then an amino acid mixture was added for 10 min (+*AA*). Cells were fixed with 4% paraformaldehyde for 15 min and permeabilized with 0.1% Triton X-100 for 5 min. ALG-2 and Sec31A were immunostained with anti-ALG-2 and anti-Sec31A antibodies, respectively, and fluorescence signals were obtained by confocal microscopy. Merged images of GFP-MISSL (*green*), ALG-2 (*cyan*), and Sec31A (*magenta*) are also shown (*Merge*). *Insets* show magnified images of the region indicated by *white squares*. *Bars,* 5 μm.

were found to be appropriate for observing the accurate localization of endogenous MISSL, and we monitored GFP-MISSL instead. Under the amino acid-starved condition, GFP-MISSL showed a mostly dispersed distribution throughout the cells and faint dots, yet it colocalized with ALG-2 (Fig. 3*E*, −*AA*). ALG-2 was stained as a punctate pattern even in the amino acid-starved condition (Fig. 3*E*, −*AA*), slightly different from live cell imaging. This might be due to fixation and permeabilization procedures in the immunostaining, *i.e.* cytosolic fraction of ALG-2 might be washed out, and therefore smaller pools of ALG-2 dots could become remarkable. Upon amino acid supplementation, GFP-MISSL puncta were apparent, and these puncta were significantly colocalized with endogenous ALG-2 (Fig. 3*E*, +*AA*), consistent with the live cell imaging. MISSL tagged with either Myc at the N terminus or GFP at the C terminus also showed similar colocalization with ALG-2 (data not shown). Furthermore, most of the GFP-MISSL puncta also colocalized with Sec31A (Fig. 3*E*, +*AA*) but not with LAMP1 (a lysosome marker) or EEA1 (an early endosome marker) (supplemental Fig. S1). Although ALG-2 strongly binds to Sec31A, we were unable to detect a ternary complex composed of MISSL, ALG-2, and Sec31A through immunoprecipitation (Fig. 1*B*), suggesting that MISSL localizes at the ERES upon calcium rise but binds to a subpopulation of ALG-2 that is not associated with Sec31A.

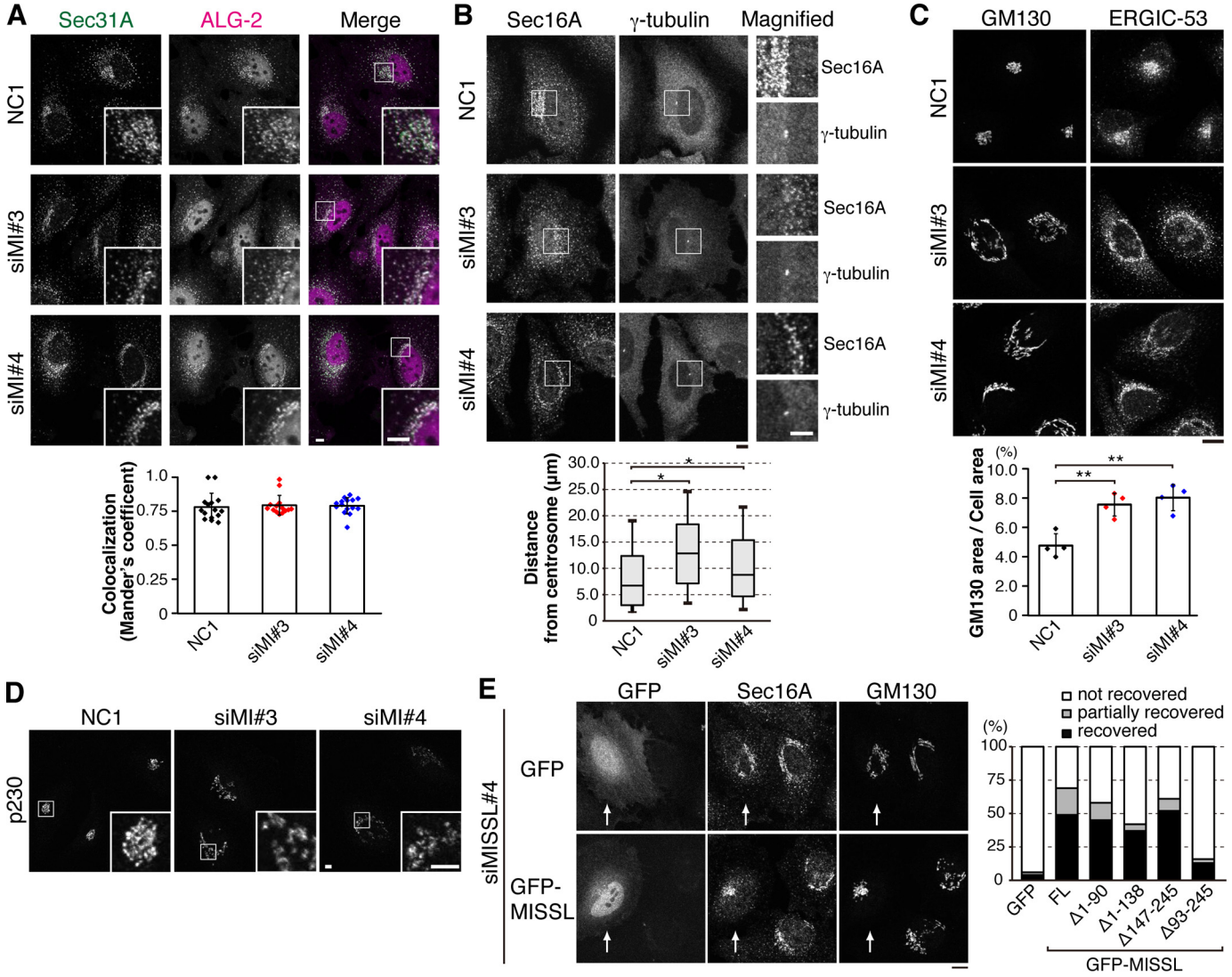

Figure 4. Knockdown of MISSL affects the localization of ERES and ERGIC components. *A, top panel,* HeLa cells were transfected with control siRNA (*NC1*) or two different siRNAs for MISSL (*siMI#3* and *siMI#4*). After 48 h, the cells were fixed with 4% paraformaldehyde, permeabilized with 0.1% Triton X-100, and then immunostained with indicated antibodies. Merged images of Sec31A (*green*) and ALG-2 (*magenta*) are also shown (*Merge*). *Insets* show magnified images of the region indicated by white squares. *Bars,* 5 μm. *Bottom panel,* Mander's correlation coefficient between ALG-2 and Sec31A was graphed as mean ± S.D. ($n = 15$). *B, top panel,* HeLa cells were treated as in *A* and immunostained with Sec16A and γ-tubulin for the ERES and the centrosome, respectively. Magnified images of the region indicated by a *white square* are also shown. *Bars,* 5 μm. *Bottom panel,* individual distances of Sec16A-positive dots from the centrosome were measured from 15 cells for NC1- and siMISSL#4-treated cells and from 14 cells for siMISSL#3-treated cells, and they are represented by *box and whisker plots*. The *boxes* denote the 25th to 75th percentile with a *line* at the median, and *whiskers* denote the 10th to 90th percentile. *, $p < 0.05$. *C, top panel,* HeLa cells were treated as in *A*. *Bar,* 10 μm. *Bottom panel, cis*-Golgi area relative to the cell volume was calculated and represented as mean ± S.D. from four independent experiments. **, $p < 0.01$. *D,* HeLa cells were treated as in *A* and immunostained with an antibody for p230, a *trans*-Golgi marker. *Insets* show magnified images of the region indicated by *white squares*. *Bars,* 5 μm. *E,* HeLa cells that were transfected with siRNA for MISSL (*siMISSL#4*) for 24 h were then transfected with the expression plasmid for GFP or GFP-MISSL for 24 h, treated as in *A*, and immunostained with anti-Sec16A and anti-GM130 antibodies. Knockdown with siMISSL#4 targets the sequence in the 3′-untranslated region (*UTR*) of human MISSL and therefore does not affect expressions of GFP-MISSL constructs, which lack 3′UTR. The transfected cells are shown by *arrows*. *Bar,* 10 μm. The percentages of the recovery of the perinuclear localization of both Sec16A and GM130 (*recovered*) or that of either protein (*partially recovered*) upon expression of GFP, full-length GFP-MISSL (*FL*), or GFP-MISSL deletion mutants are also shown (GFP, $n = 51$; GFP-MISSL FL, $n = 45$; GFP-MISSLΔ1–90, $n = 53$; GFP-MISSLΔ1–138, $n = 43$; GFP-MISSLΔ147–245, $n = 44$; GFP-MISSLΔ93–245, $n = 39$).

MISSL regulates the proper distribution of the components of ERES, ERGIC, and Golgi

Several lines of evidence have suggested that ALG-2 plays a role in ER-to-Golgi vesicular trafficking and that ALG-2 depletion or specific disruption of the interaction between ALG-2 and Sec31A causes redistribution of the ER-to-Golgi components (7, 16). Therefore, we examined the effect of MISSL depletion on the ER-to-Golgi compartment by indirect immunofluorescence. First, Sec31A and ALG-2 were immunostained in HeLa cells. In control cells, the immunofluorescence signal from the Sec31A antibody displayed staining of the peripheral region of the nucleus. In contrast, depletion of MISSL mediated by two different siRNAs caused dispersed localization of Sec31A (Fig. 4*A*). ALG-2 also showed slight relocalization and dispersed staining, but most of ALG-2 was still colocalized with Sec31A at a level comparable with that in control cells, as indicated by the colocalization index (Fig. 4*A*, *lower panel*). To determine whether the distribution of ERESs was altered, we stained Sec16A, another ERES marker. Again, Sec16A staining peripheral to the nucleus in control cells was disturbed upon

MISSL knockdown (Fig. 4*B*). Quantification of the distance between Sec16A-positive dots and the centrosome marked by γ-tubulin showed that the increase in the distance between Sec16A and the centrosome was statistically significant (Fig. 4*B*, *lower panel*), indicating the redistribution of Sec16A-positive dots close to the nucleus toward the peripheral region of the cells. Concomitant with the Sec31A and Sec16A disturbance, ERGIC-53, an ERGIC marker, and GM130, a *cis*-Golgi marker, also showed aberrant distribution upon MISSL knockdown (Fig. 4*C*), whereas the expression of these proteins was not significantly altered (supplemental Fig. S2). Quantification of the ratio of the GM130-staining area to the cell volume indicated a 1.6–1.8-fold expansion upon MISSL knockdown (Fig. 4*C*, *lower panel*). Moreover, MISSL knockdown also caused aberrant distribution of p230, a *trans*-Golgi marker (Fig. 4*D*), suggesting the altered distribution of Golgi compartments. To further examine whether altered distributions of Sec16A and GM130 were dependent on the ability of MISSL to bind to ALG-2, we reintroduced GFP, GFP-MISSL, or GFP-MISSL deletion mutants. The aberrant distributions of Sec16A and GM130 were significantly recovered by reintroduction of GFP-MISSL but not GFP (Fig. 4*E*), although those were not fully recovered by GFP-MISSL most likely due to partial cellular damages during siRNA-mediated knockdown followed by transfection procedures. Nonetheless, GFP-MISSLΔ147–245, which failed to bind to ALG-2 (Fig. 1), was able to recover the aberrant distributions of Sec16A and GM130 to some extent (Fig. 4*E*, *graph*), suggesting that altered distributions of these compartments appear to be caused by the loss of MISSL function different from binding to ALG-2. Consistent with this, it was reported that knockdown of ALG-2 did not affect the Golgi organization (16). Together, these results suggest that MISSL knockdown induces rearrangement of the ERES, ERGIC, and Golgi compartments and that MISSL likely plays a role in regulation of these organelle organizations independent from its ALG-2-binding ability.

MISSL and ALG-2 regulate the secretory pathway

To investigate the role of MISSL in the secretory pathway, we monitored the secretion of secreted alkaline phosphatase (SEAP) as a model secretory protein (34–36). We examined SEAP secretion over a period of 60 min by measuring SEAP activity in the medium and in the cell-associated fraction. As expected, addition of brefeldin A (BFA), which is known to inhibit ER-to-Golgi transport, dramatically reduced the secretion of SEAP (Fig. 5*A*). Although control siRNA (NC1) treatment had no effect on the secretion of SEAP compared with mock-treated cells, knockdown of either MISSL or ALG-2 resulted in reduction of SEAP secretion by 20–40%. Furthermore, simultaneous knockdown of MISSL and ALG-2 did not have any additive effect on the reduction of SEAP secretion, although MISSL and ALG-2 were significantly depleted (Fig. 5*B*). These results suggest that MISSL and ALG-2 act in the same pathway regulating the secretion process.

Previous reports have suggested that ER stresses affect the distributions of ERES, ERGIC, and Golgi and reduce secretion (37–39), similar to the change observed upon MISSL knockdown. Thus, we measured XBP1 mRNA splicing, a known event induced during ER stresses, to determine whether MISSL knockdown induced ER stress. Neither MISSL knockdown nor ALG-2 knockdown induced XBP1 splicing in the unstressed condition (supplemental Fig. S3). Furthermore, even after DTT treatment, which induces ER stress and thereby increases XBP1 mRNA splicing, the increased levels of XBP1 mRNA splicing in MISSL and ALG-2 knockdown cells were comparable with those in mock-treated and control siRNA (NC1)-treated cells. Therefore, it is unlikely that MISSL indirectly contributes to the secretory pathway by inducing ER stress-mediated regulation.

To further examine the role of MISSL in ER-to-Golgi transport, we monitored the effect of MISSL knockdown in ER-to-Golgi transport of procollagen type I (procollagen-I), which is previously reported to be delayed by ALG-2 knockdown (28). To this end, we maintained IMR-90 cells at 40 °C to retain procollagen-I in the ER and then shifted at 32 °C to relieve export of procollagen-I. As shown in Fig. 5, *C–E*, ALG-2 knockdown delayed the procollagen-I reached at Golgi compared with mock and control siRNA (NC1)-treated cells. Strikingly, MISSL knockdown (siMISSL#3 and siMISSL#4) also consistently delayed transport of procollagen-I to Golgi. Taken together, these results suggest that MISSL and ALG-2 regulate ER-to-Golgi transport.

MISSL and ALG-2 form a complex with MAP1B

To gain an insight into the mechanism by which MISSL and ALG-2 play a role in regulation of the secretory pathway, we tried to identify novel interacting proteins. To this end, we used HeLa cells stably expressing GFP or GFP-MISSL, and the cell lysates were immunoprecipitated with the anti-GFP antibody. The immunoprecipitates were separated on SDS-PAGE and visualized by silver staining (Fig. 6*A*). Several bands specific to the immunoprecipitates from the GFP-MISSL-expressing cell lysate were cut and analyzed by liquid chromatography coupled with tandem mass spectrometry (LC-MS/MS). We identified ALG-2, which was a positive control of the analysis. Furthermore, a band with >220 kDa was identified as microtubule-associated protein 1B (MAP1B). Because the secretory pathway involves microtubules for efficient transport (40–42) and MAP1B is known to regulate microtubule dynamics in neurons (43), we focused on MAP1B for further analysis.

To confirm the interaction between MISSL, ALG-2, and MAP1B, cell lysates from HeLa cells stably expressing GFP or GFP-MISSL were immunoprecipitated with the anti-MAP1B antibody. As shown in Fig. 6*B*, GFP-MISSL, but not GFP, was specifically detected in immunoprecipitates with the anti-MAP1B antibody. Furthermore, endogenous MISSL also interacted with MAP1B (Fig. 6*C*). Addition of EGTA abolished the interaction of MAP1B with MISSL and ALG-2 (Fig. 6, *B* and *C*), suggesting that MISSL, ALG-2, and MAP1B form a complex in a calcium-dependent manner. Because Sec31A, a strong binding partner of ALG-2, did not bind to MAP1B (Fig. 6*C*), MAP1B appears to selectively bind to a subpopulation of ALG-2, including MISSL. Although MAP1B was identified as an MISSL-binding protein (Fig. 6*A*), the fraction of ALG-2 associated with MAP1B was larger than that of MISSL, and the formation of a ternary complex was calcium-dependent, implying that MISSL binds to MAP1B through ALG-2. To further examine whether

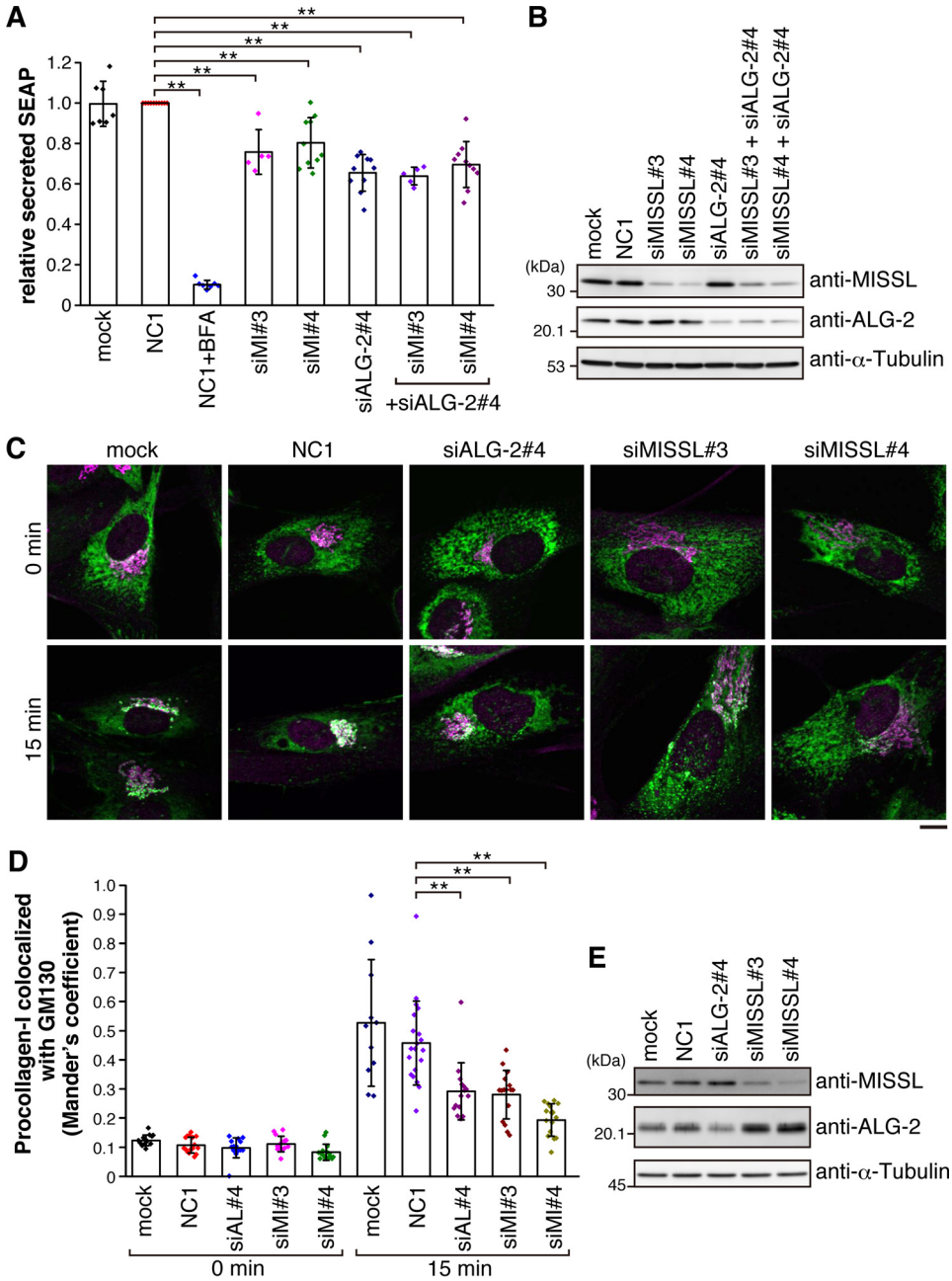

Figure 5. MISSL and ALG-2 are involved in proper secretion. *A,* HeLa cells stably expressing SEAP were transfected with siRNAs for a control (*NC1*), for MISSL (*siMI#3* and *siMI#4*), or for ALG-2 (*siALG-2#4*) or were not transfected with siRNA (*mock*). After 48 h, the cells were washed once with media and then incubated for 60 min in fresh media. SEAP activity in media and cellular SEAP activity were measured, and the ratio of secreted SEAP activity to cellular SEAP activity was calculated as secreted SEAP. Data are represented as relative secreted SEAP, which was normalized to the secreted SEAP in the control (*NC1*). Data are shown as mean ± S.D. BFA was also included as a positive control for the inhibition of secretion. Biological replicates are as follows: NC1 ($n = 10$); mock ($n = 7$); NC1+BFA ($n = 7$); siALG-2#4 ($n = 10$); siMI#3 ($n = 5$); siMI#4 ($n = 10$); siALG-2#4+siMI#3 ($n = 5$); and siALG-2#4+siMI#4 ($n = 10$). **, $p < 0.01$. *B,* HeLa cells were transfected with the indicated siRNAs. The cell lysates were analyzed by immunoblotting with the indicated antibodies. *C,* IMR-90 cells were incubated at 40 °C for 3 h and then were shifted to 32 °C to promote procollagen-I export for 15 min. The cells were fixed and immunostained with anti-procollagen-I (*green*) and anti-GM130 (*magenta*) antibodies. Representative merged images are shown. *Bar,* 10 μm. *D,* Mander's correlation coefficient between procollagen-I and GM130 at 0 and 15 min of export was graphed as mean ± S.D. Numbers of cells analyzed were as follows: mock 0 min ($n = 14$), NC1 0 min ($n = 16$), siALG-2#4 0 min ($n = 14$), siMISSL#3 0 min ($n = 14$), siMISSL#4 0 min ($n = 15$), mock 15 min ($n = 11$), NC1 15 min ($n = 20$), siALG-2#4 15 min ($n = 15$), siMISSL#3 15 min ($n = 16$), and siMISSL#4 15 min ($n = 15$). **, $p < 0.01$. *E,* IMR-90 cells were transfected with indicated siRNAs. The cell lysates were analyzed by immunoblotting with the indicated antibodies.

ALG-2 mediates the association between MISSL and MAP1B, we constructed ALG-2 knock-out (KO) HeLa cells stably expressing GFP or GFP-MISSL. In the ALG-2 KO cells, GFP-MISSL was not coimmunoprecipitated with MAP1B (Fig. 6*D*). Furthermore, the interactions between ALG-2 and MAP1B were not reduced in MISSL KO cells (Fig. 6*E*). These results suggest that ALG-2 mediates the association between MISSL and MAP1B and that binding of ALG-2 to MAP1B is independent from MISSL binding to ALG-2.

To further examine whether ALG-2 colocalized with MAP1B, HeLa cells were immunostained with anti-ALG-2 and anti-MAP1B antibodies. In the formaldehyde-fixed condition,

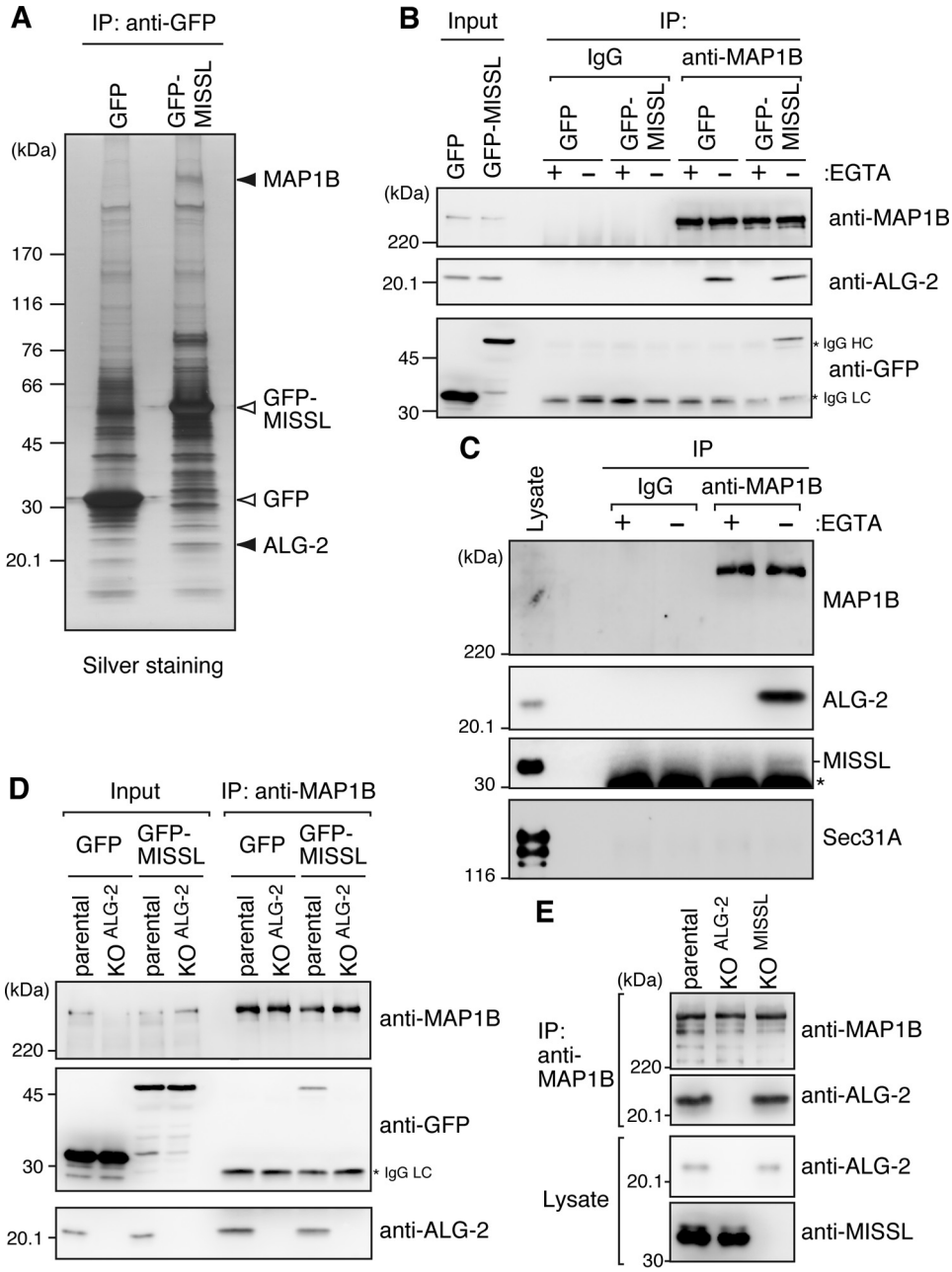

Figure 6. MAP1B associates with ALG-2 and MISSL in a calcium-dependent fashion. *A,* cell lysates prepared from HeLa cells stably expressing GFP or GFP-MISSL were subjected to IP with GFP-TrapA. The immunoprecipitates were resolved by 4–20% gradient SDS-PAGE followed by silver staining. MAP1B and ALG-2 (indicated by *filled triangles*) were identified by LC-MS/MS. The bands corresponding to GFP and GFP-MISSL are also shown (*open triangles*). *B,* lysates from HeLa cells stably expressing GFP or GFP-MISSL were subjected to IP with control IgG or the anti-MAP1B antibody in the presence (+) or absence (−) of EGTA. The immunoprecipitates were analyzed by immunoblotting using indicated antibodies. An *asterisk* indicates IgG heavy chain (*HC*) and light chain (*LC*). Cell lysates (*Input*) corresponding to 2% for anti-MAP1B and 0.5% for anti-ALG-2 and anti-GFP antibodies were also loaded. *C,* HeLa cell lysates were subjected to IP with control IgG or the anti-MAP1B antibody in the presence (+*EGTA*) or absence of EGTA. The presence of indicated proteins in the immunoprecipitates was analyzed by immunoblotting. An *asterisk* indicates IgG light chain. The cell lysates (*Lysate*) correspond to 0.5% of respective immunoprecipitates. *D,* lysates from HeLa cells (*parental*) or ALG-2 KO cells (KO^{ALG-2}) stably expressing GFP or GFP-MISSL were subjected to IP with the anti-MAP1B antibody. The immunoprecipitates were analyzed by immunoblotting using indicated antibodies. Cell lysates (*Input*) corresponding to 7% for anti-MAP1B and 1% for anti-ALG-2 and anti-GFP antibodies were also loaded. *E,* lysates from HeLa cells (*parental*), ALG-2 KO cells (KO^{ALG-2}) or MISSL KO cells (KO^{MISSL}) were subjected to IP with the anti-MAP1B antibody. The immunoprecipitates were analyzed by immunoblotting using indicated antibodies.

MAP1B localized diffusely throughout the cytoplasm (data not shown), as reported previously (44), and we alternatively used methanol fixation. Although the anti-MAP1B antibody used showed nuclear staining, the cytoplasmic microtubule-like staining by the anti-MAP1B antibody could indeed detect endogenous MAP1B localization as validated by using MAP1B KO HeLa cells (supplemental Fig. S4). As shown in Fig. 7, *A* and *B*, in methanol fixation ALG-2 also showed microtubule-like staining, which was colocalized with MAP1B, in addition to larger dots colocalized with Sec31A. Further analyses of signals corresponding to ALG-2, MAP1B, and Sec31A (Fig. 7, *C* and *D*) suggested three types of colocalization as follows: the colocalization of ALG-2 with both MAP1B and Sec31A (*arrow*); the colocalization of ALG-2 with MAP1B but not Sec31A (*arrow-*

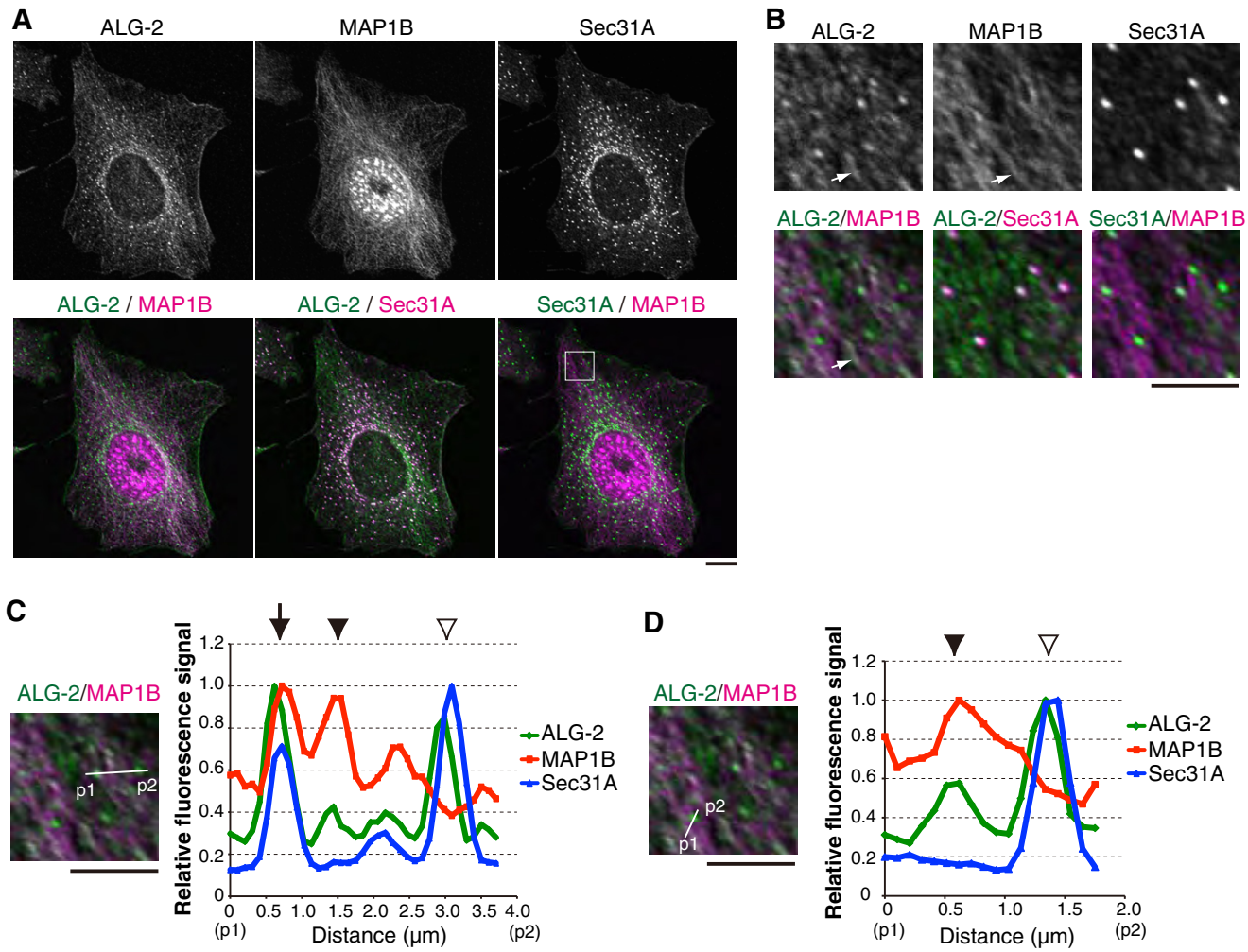

Figure 7. ALG-2 partially colocalizes with MAP1B. *A,* HeLa cells were fixed with methanol and were immunostained with the indicated antibodies. *Bar,* 5 μm. *B,* magnified images of the region indicated by a *white square* in *A* are shown. *White arrows* indicate representative ALG-2 located along MAP1B. *Bar,* 5 μm. *C* and *D,* fluorescence signal intensities of ALG-2, MAP1B, and Sec31A along lines (*p1* to *p2*) were measured using ImageJ and plotted. Respective fluorescence intensities were represented as the fluorescence intensities relative to the respective maximal value. An *arrow* indicates the colocalization of ALG-2 with MAP1B and Sec31A. *Arrowheads* and *open arrowheads* indicate the colocalization of ALG-2 with MAP1B and the colocalization of ALG-2 with Sec31A, respectively. *Bars,* 5 μm.

heads); and the colocalization of ALG-2 with Sec31A but not MAP1B (*open arrowheads*). The ratio of colocalization of the three proteins to the colocalization of ALG-2 and Sec31A was less frequent (19.8% from two independent experiments and 637 dots analyzed). Unfortunately, we were currently unable to observe the exact localization of GFP-MISSL in the methanol-fixed condition, most likely due to the inaccessibility of anti-GFP antibodies. Consistent with biochemical analyses, these results suggested that ALG-2 partially associates with MAP1B in the cells.

Knockdown of MAP1B complements the reduced secretion caused by MISSL and ALG-2 depletion

Because knockdown of either MISSL or ALG-2 resulted in reduced secretion of SEAP (Fig. 5*A*), we tested the effect of MAP1B knockdown on the secretion. MAP1B was efficiently depleted in HeLa cells without affecting MISSL and ALG-2 expression (Fig. 8*A*). In the secretion assay using SEAP, the depletion of MAP1B alone did not affect the secretion (Fig. 8*B*). In contrast, the depletion of MAP1B could rescue the reduced secretion of SEAP by either MISSL or ALG-2 depletion to a level similar to that in control cells (Fig. 8*B*). These results suggest that MAP1B specifically acts downstream of MISSL and ALG-2 in the secretion process.

Discussion

Our results demonstrated that ALG-2 regulates the secretory pathway via interaction with both MISSL, a previously uncharacterized protein, and MAP1B. Because depletion of MAP1B could revert the reduced secretion caused by MISSL or ALG-2 depletion (Fig. 8*B*) and ALG-2 bridges MISSL and MAP1B in the presence of calcium (Fig. 6, *B–D*), we speculate that the binding of MISSL and ALG-2 likely inhibits MAP1B action, thereby leading to the calcium-dependent fine-tuning of the secretory pathway in response to cellular and environmental demands (Fig. 8*C*). Thus, our findings provide a new insight into the molecular mechanism of ALG-2-dependent calcium signaling that regulates the secretory pathway by the MISSL–ALG-2–MAP1B complex identified in this study in addition to the Sec31A–ALG-2–annexin A11 complex as shown previ-

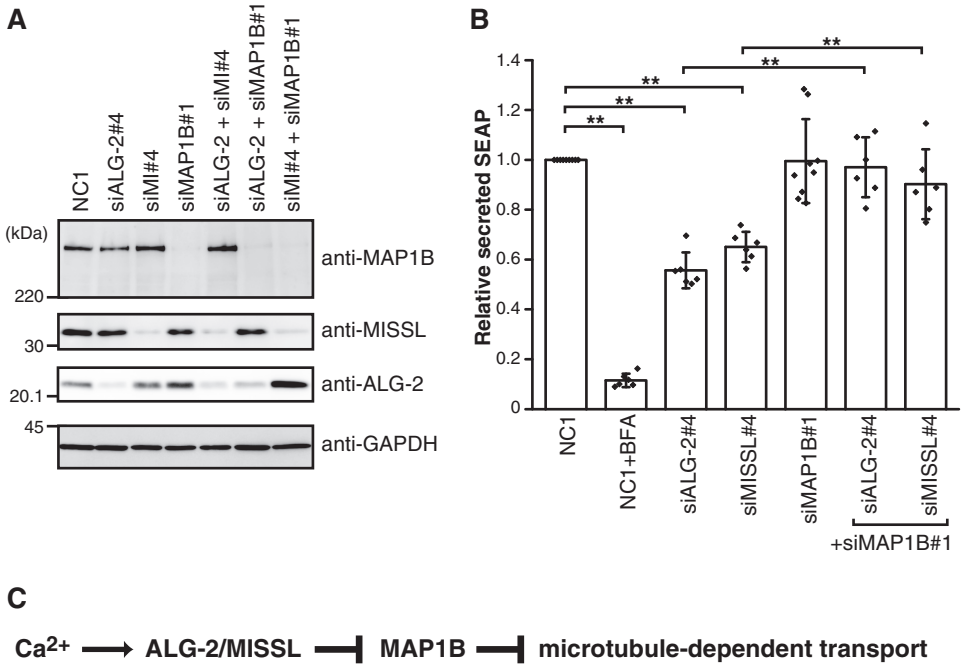

Figure 8. MAP1B knockdown recovers the reduced secretion caused by MISSL and ALG-2 depletion. *A,* HeLa cells were transfected with siRNAs for a control (*NC1*), for MISSL (*siMI#4*), for ALG-2 (*siALG-2#4*), or for MAP1B (*siMAP1B#1*). After 48 h, the cell lysates were analyzed by immunoblotting using the indicated antibodies. *B,* HeLa cells stably expressing SEAP were transfected with siRNAs for a control (*NC1*), for MISSL (*siMI#4*), for ALG-2 (*siALG-2#4*), or for MAP1B (*siMAP1B#1*). After 48 h, the cells were washed once with media and then incubated for 60 min in fresh media. Both SEAP activity in media and cellular SEAP activity were measured, and the ratio of secreted SEAP activity to cellular SEAP activity was calculated as secreted SEAP. Data are represented as the relative secreted SEAP, which was normalized to the secreted SEAP in the control (*NC1*). BFA was also included as a positive control for the inhibition of secretion. Data are shown as mean ± S.D. Biological replicates are as follows: NC1 ($n = 9$); NC1+BFA ($n = 6$); siALG-2#4 ($n = 6$); siMI#4 ($n = 6$); siMAP1B#1 ($n = 9$); siALG-2#4+siMAP1B#1 ($n = 6$); and siMI#4+siMAP1B#4 ($n = 6$). **, $p < 0.01$. *C,* model for ALG-2-MISSL-MAP1B ternary complex-mediated regulation of transport. See text for details.

ously (16). These two modes of regulation highlight the importance of the calcium/ALG-2-mediated fine-tuning of the secretory pathway.

MAP1B expression is developmentally regulated and is high in neurons (43). In neurons, MAP1B was shown to regulate microtubule dynamics (45, 46). MAP1B binds to dynamic microtubules rather than stable microtubules (47) and also regulates the stability of microtubules (48). Although MAP1B expression in HeLa cells appears to be relatively low, our findings suggest that MAP1B is important for the regulation of secretion that relies on ALG-2 and MISSL in non-neuronal cells.

Previous reports have indicated that ER-to-Golgi transport along microtubules at least in part depends on the direct interaction between Sec23, the inner coat component of COPII, and the dynein-dynactin complex (41). Dynein and MAP1B share similar microtubule-binding motifs (49), and MAP1B association to microtubules was reported to interfere with the binding of dynein (50, 51), like other microtubule-associated proteins such as Tau and MAP2 (52). MAP1B was also reported to bind to Lis1, a regulator of dynein (53, 54), and to affect the binding of Lis1 with dynein (55). Thus, it is likely that the binding of MISSL with MAP1B through the ALG-2 adaptor function may prevent binding of MAP1B to microtubules, thereby allowing the binding of dynein with microtubules to accelerate ER-to-Golgi transport. A global or local calcium rise, which is beneficial for efficient transport (5–7), might affect the access of MAP1B to microtubules via ALG-2 and MISSL. In contrast, under an ALG-2 or MISSL-depleted condition, MAP1B can bind to microtubules and inhibit dynein binding to microtubules and/or dynein movement. This scenario is also consistent with the lack of an effect of single MAP1B knockdown on the secretion of SEAP, when MAP1B action was already inhibited by MISSL and ALG-2. Because MAP1B is phosphorylated by several kinases such as GSKβ and casein kinase II and the phosphorylation status is involved in the maintenance of a stable/dynamic microtubule population (48), it is possible that MISSL and ALG-2 binding to MAP1B contributes to the post-translational modifications of MAP1B. Very recently, ALG-2 was shown to bind to α-tubulin and was suggested to regulate microtubule dynamics in an unknown fashion (56, 57). Although the detailed mechanism of ALG-2 action on microtubule dynamics remains unknown, ALG-2 might regulate these intracellular events through binding to MAP1B and MISSL.

We showed that MISSL and MAP1B bind to ALG-2 in a calcium-dependent fashion. Although MISSL contains ABM-1-like motifs, they were not essential for binding with ALG-2 (Fig. 1), and our results suggested that MISSL likely binds to ALG-2 through multiple regions. Because MISSL is composed of proline-rich sequences (34% for proline residues in the whole region) and ALG-2 preferentially binds to ABM-1 and ABM-2 in the proline-rich regions, multiple interactions may support the overall binding ability between MISSL and ALG-2. Previous results indicate that the splicing isoform of ALG-2 lacking ^{121}GF^{122} (ALG-2ΔGF) fails to bind to proteins containing ABM-1 (17, 33, 58). Because MISSL could not bind to ALG-2ΔGF in a pulldown assay (data not shown), MISSL binding to

ALG-2 most likely involves the ABM-1-like binding mode, which requires formation of the ALG-2 homodimer, suggesting that the ALG-2 homodimer acts as an adaptor that bridges MISSL and MAP1B. In contrast, it remains unknown how MAP1B binds to ALG-2, due to the lack of apparent ABM-1 and ABM-2. It is possible that ALG-2 interacts with MAP1B through a distinct binding mode involving novel interacting motifs.

We previously demonstrated that ALG-2 bridges Sec31A and annexin A11 to regulate ER-to-Golgi transport, possibly by stabilizing the Sec31A turnover to ERES (16). In contrast, ALG-2 is unable to link MISSL with Sec31A and annexin A11 (Fig. 1*B*, and data not shown). Furthermore, Sec31A was excluded in the MISSL–ALG-2–MAP1B complex (Fig. 6*C*). These results suggest that the MISSL–ALG-2–MAP1B complex identified in this study exists as functionally distinct machinery from the Sec31A–ALG-2–annexin A11 complex. Thus, ALG-2 likely plays a role in the proper control of ER-to-Golgi transport through formation of these two types of distinct complex in response to the cellular status or demand.

Our results showing that MISSL knockdown causes dramatic changes in the localization of ERES (Sec31A and Sec16A), ERGIC (ERGIC-53), and Golgi (GM130 and p230) suggest that MISSL also functions as a modulator of the organization of these compartments. Because GFP-MISSLΔ147–245, but not GFP-MISSLΔ93–245, could rescue aberrant localizations of Sec16A and GM130 to some extent (Fig. 4*E*), a region spanning 93–146 amino acids might be responsible for their proper distribution. It is possible that the change in secretion rate results from alteration in the organization of ERES and Golgi. However, the reduction of secretion by MISSL depletion is unlikely to be due to the disorganization of ERES, ERGIC, and Golgi *per se* because MAP1B depletion could fully rescue the reduced secretion (Fig. 8*B*) but not the localization of these compartments (data not shown). These results also suggest that MISSL has an additional function regulating the localization of these organelles other than the MISSL–ALG-2–MAP1B complex. It is currently unknown which compartment is a primary defect upon MISSL depletion, because localization of these organelles is interdependent. However, given the GFP-MISSL localization at the ERES, it is likely that MISSL primarily contributes to the proper organization of ERES.

In summary, identification of the novel calcium-dependent complex MISSL–ALG-2–MAP1B will expand the importance of ALG-2 sensor function and provide a molecular framework for the complex regulation of secretory pathways that are necessary for the proper adaptation of dynamic cellular and environmental changes.

Experimental procedures

Antibodies and reagents

Anti-GFP (B-2, sc-9996), anti-MISSL (C-16, sc-243408), anti-MAP1B (N-19, sc-8970), anti-MAP1B (H-8, sc-365668), anti-Sec23 (E-19, sc-12107), and anti-GAPDH (6C5, sc-32233) antibodies were purchased from Santa Cruz Biotechnology (Dallas, TX). Anti-MISSL (HPA034506), anti-ERGIC53 (E1031), anti-α-tubulin (DM1A), and anti-γ-tubulin (GTU88) antibodies were from Sigma. Anti-Sec16A (A300–648A) was from Bethyl Laboratories (Montgomery, TX). Anti-GM130 (clone 35), anti-p230 *trans*-Golgi (clone 15), anti-EEA1 (clone 14), and anti-LAMP1 (H4A3) antibodies were from BD Transduction Laboratories (San Jose, CA). The anti-procollagen type I C-peptide antibody (clone PC5–5) was purchased from Takara (Shiga, Japan). The anti-GM130 rabbit polyclonal antibody (PM061) was purchased from MBL (Nagoya, Japan). Rabbit polyclonal antibodies against ALG-2 and Sec31A and a goat polyclonal antibody against ALG-2 were produced as described previously (13, 29). Horseradish peroxidase (HRP)-conjugated goat antibodies against mouse IgG and rabbit IgG and an HRP-conjugated rabbit antibody against goat IgG were from Jackson ImmunoResearch (West Grove, PA). For immunofluorescence, AlexaFluor488-, AlexaFluor555-, or AlexaFluor647-conjugated donkey anti-mouse IgG, AlexaFluor488-, AlexaFluor555-, or AlexaFluor647-conjugated donkey anti-rabbit IgG, and AlexaFluor488-, AlexaFluor555-, or AlexaFluor647-conjugated donkey anti-goat IgG antibodies were purchased from Invitrogen and used as secondary antibodies. Thapsigargin (TG) and brefeldin A (BFA) were purchased from Wako (Tokyo, Japan).

Expression plasmids

To create expression plasmids for GFP-MISSLΔ1–90, GFP-MISSLΔ147–245, GFP-MISSLΔ93–245, and GFP-MISSLΔ1–138, pEGFP-C3-MISSL (pEGFP-C3-MISSL was previously designated MISS but renamed MISSL in this article according to the change of nomenclature under UniProt Q8NDC0) (29) was digested with BamHI, BspEI and SalI, BspEI and ScaI, and EcoRI and PstI, respectively, followed by blunt-ending and ligation. The expression plasmid for GFP-MISSLΔΔ was generated by site-directed mutagenesis using a primer set (5′-CCCCAC-CTGGTGGTACACCAAATATGCC-3′, 5′-GGCATATTTG-GTGTACCACCAGGTGGGG-3′, 5′-CTACCCCTAATATG-GCTCCTCCTCCTCC-3′, and 5′-GGAGGAGGAGGA-GCCATATTAGGGGTAG-3′) and PrimeSTAR Max DNA polymerase (Takara). The sequences of plasmids were verified by DNA sequencing. To create a retrovirus vector for EGFP-MISSL, pEGFP-C3-MISSL was digested with AgeI and SalI, and the DNA fragment containing EGFP-MISSL was ligated into the BspEI and MluI sites of pCX4pur (59).

The plasmids encoding Cas9 (pSpCas9(BB)-2A-puro(PX459) V2.0, Addgene plasmid no. 62988 (60)) and Cas9 with improved specificity (61) (eSpCas9(1.1), Addgene plasmid no. 71814) were gifts from Dr. Feng Zhang. To create an eCas9 expression plasmid (eSpCas9(1.1)-2A-puro) that possesses the puromycin-resistant gene cassette, pSpCas9(BB)-2A-puro was digested with FseI and NotI, and the DNA fragment containing the puromycin-resistant gene region was inserted into the FseI and NotI sites of eSpCas9(1.1). To generate a plasmid (eSpCas9(1.1)-2A-puro/ALG-2) used for generation of human ALG-2 knock-out cells, primers hALG-2 sgRNA-top (5′-caccgagggccggggcggtaagagt-3′) and hALG-2 sgRNA-bottom (5′-aaacactcttaccgccccggccctc-3′) were annealed and then ligated into the BbsI site of eSpCas9(1.1)-2A-puro. Similarly, primers hMISSL sgRNA-top (5′-caccggagcctggccagccttgagg-3′) and hMISSL sgRNA-bottom (5′-aaaccctcaaggctggccaggctcc-3′) or primers hMAP1B sgRNA-top (5′-caccgtgttgccgatggcacgccgc-

3′) and hMAP1B sgRNA-bottom (5′-aaacgcggcgtgccatcggcaacac-3′) were annealed and ligated into BbsI sites of eSpCas9(1.1)-2A-puro to construct plasmids (eSpCas9(1.1)-2A-puro/MISSL or eSpCas9(1.1)-2A-puro/MAP1B) used for generation of human MISSL or MAP1B knock-out cells.

The expression plasmid for mCherry-ALG-2 (pmCherry-C1/ALG-2) was described previously (62). The expression plasmid for R-GECO1 (CMV-R-GECO1) (31) was a gift from Dr. Robert Campbell (Addgene plasmid no. 32444).

Mammalian cell culture, transfection, and retroviral infection

HEK293T, HeLa, and IMR-90 (normal lung fibroblast) cells were grown at 37 °C in Dulbecco's modified Eagle's medium (DMEM) with 1,000 mg/liter glucose (Nissui) supplemented with 10% fetal bovine serum under a 5% CO_2 atmosphere. HeLa cells stably expressing SEAP (36) were a kind gift from Dr. Ayano Satoh (Okayama University). Transient transfection of the indicated plasmids was performed using the calcium phosphate method for HEK293T cells and FuGENE 6 (Promega, Madison, WI) for HeLa cells according to the manufacturer's instructions. HeLa cells stably expressing EGFP or EGFP-MISSL were generated by retroviral infection essentially as described previously (63). Retroviruses were prepared from culture media of PLAT-A cells (64) (kindly provided by Dr. Toshio Kitamura, University of Tokyo) that had been transfected with pCX4pur-EGFP-C1 (laboratory stock) or pCX4pur-EGFP-MISSL using FuGENE 6.

Amino acid starvation and readdition were done as described before (65) with modifications. In brief, cells were washed once with Hanks' balanced salt solution (HBSS) and incubated in HBSS for 50–60 min. For replenishment of amino acids, an amino acid mixture was added at the following final concentrations (mg/liter): L-Arg, 84; L-Cys, 48; L-His, 84; L-Ile, 105; L-Leu, 105; L-Lys, 145; L-Met, 30; L-Phe, 66; L-Thr, 95; L-Trp, 20; L-Tyr, 72; L-Val, 94; L-Gln, 584.

Generation of ALG-2, MISSL, and MAP1B knock-out HeLa cells

Generation of ALG-2, MISSL and MAP1B knock-out HeLa cells by the CRISPR/Cas9 system was done as described previously (60). Briefly, HeLa cells were transfected with the plasmid (eSpCas9(1.1)-2A-puro/ALG-2, eSpCas9(1.1)-2A-puro/MISSL or eSpCas9(1.1)-2A-puro/MAP1B) using FuGENE 6. After 24 h, cells were selected with 1 μg/ml puromycin for 3 days to remove untransfected cells. Then the cells were plated on 96-well plates in media without puromycin, and single colonies were selected. ALG-2, MISSL, or MAP1B knock-out cells were identified by Western blotting with anti-ALG-2, anti-MISSL, and anti-MAP1B antibodies, respectively.

Small interfering RNA (siRNA)-mediated RNA interference

HeLa cells were transfected with Dicer-substrate siRNAs (DsiRNAs) (Integrated DNA Technologies, Coralville, IA) using the Lipofectamine RNAiMax reagent (Invitrogen) according to the manufacturer's instruction. The following DsiRNAs, which were composed of RNA and DNA, with the sense strand sequences indicated were used: negative control (NC1, 5′-cguuaaucgcguauaauacgcguAT-3′, DNA parts shown in uppercase); human ALG-2 (siALG-2#4, 5′-aaagacaggaguggagugauaucAG-3′); human MISSL (siMISSL#3, 5′-ugaaccucaaacuagauaaacccTA-3′; siMISSL#4, 5′-accucucagagaagauaacugccTC-3′); and human MAP1B (siMAP1B#1, 5′-gucauugugacgccaaugaauuuCA-3′).

Cell lysate preparation and immunoprecipitation

HeLa cells grown on a 100-mm dish were washed once with ice-cold PBS and lysed with 1 ml of lysis buffer A (40 mM HEPES-NaOH (pH 7.5), 120 mM NaCl, 0.3% CHAPS, 50 mM NaF) containing 3 μg/ml leupeptin, 1 μM pepstatin A, and 0.1 mM Pefabloc. In Fig. 6, lysis buffer A containing 9 μg/ml leupeptin, 3 μM pepstatin A, and 0.3 mM Pefabloc was used for cell lysis. After centrifugation at 9,000 × *g* for 10 min, the supernatant was incubated with anti-MISSL or anti-MAP1B antibody in the absence or presence of 100 μM $CaCl_2$ or 5 mM EGTA overnight. The immunocomplexes were collected by the addition of Dynabeads protein G (Invitrogen) and washed three times with the respective buffer conditions used for incubation with the antibody. In Fig. 1, *A*, *D*, and *F*, after 24–48 h of transfection the cells were lysed with buffer A containing 3 μg/ml leupeptin, 1 μM pepstatin A, and 0.1 mM Pefabloc and centrifuged at 9,000 × *g* for 10 min. The cell lysates were incubated with GFP-TrapA (Chromotek, Planegg-Martinsried, Germany) for 3 h in the absence or presence of 100 μM $CaCl_2$ or 5 mM EGTA and washed three times as above.

Far-Western blotting

Far-Western blotting using biotin-labeled ALG-2 as a probe was carried out essentially as described previously (29). After 24 h of transfection, cells were lysed with lysis buffer B (50 mM Tris-HCl (pH 7.5), 150 mM NaCl, 0.2% Triton X-100) containing 3 μg/ml leupeptin, 1 μM pepstatin A, and 0.1 mM Pefabloc. After centrifugation at 9,000 × *g* for 10 min, the supernatant was incubated with GFP-TrapA for 3 h. Immunoprecipitates were resolved by SDS-PAGE and incubated with biotin-labeled ALG-2 in the presence of 100 μM $CaCl_2$ or with anti-GFP antibody.

Live-cell imaging

Live-cell imaging analyses were done essentially as described previously (16, 62). Briefly, HeLa cells were seeded in a glass-bottom dish (Asahi Glass, Tokyo, Japan) and were transiently transfected with expression vectors. After 24 h, cells were then treated as follows. For amino acid starvation, the medium was replaced with HBSS for 60 min. Time-lapse images were acquired under an FV1000-D confocal laser-scanning microscope equipped with a 1.35 numerical aperture oil-immersion objective (UPLSAPO60XO, Olympus, Tokyo, Japan) before and after addition of an amino acid mixture at 37 °C. For TG treatment, the medium was replaced with Leibovitz's L15 medium (Invitrogen) containing 1% fetal bovine serum, and then TG was added at the final concentration of 2 μM.

Indirect immunofluorescence

HeLa cells were seeded onto cover glasses and transfected with siRNAs. After 48–72 h, the cells were washed once with PBS(−) and fixed with 4% PFA/PBS(−) for 15 min, followed by washing three times with PBS(−). Then the cells were permea-

bilized with 0.1% Triton X-100/PBS(−) for 5 min, followed by washing three times with PBS(−). After blocking with 0.1% gelatin/PBS(−) for 60 min, the cells were incubated with primary antibodies at 4 °C overnight and washed five times with 0.1% gelatin/PBS(−). Cell were then incubated with secondary antibodies at room temperature for 60 min in the dark and then washed five times with 0.1% gelatin/PBS(−) and mounted. Images were acquired under an FV1000-D confocal laser-scanning microscope.

For detection of colocalization between ALG-2, MAP1B, and Sec31A (Fig. 7), HeLa cells were washed once with PBS(−) and fixed with prechilled methanol at −20 °C for 15 min, followed by washing three times with PBS(−). For the procollagen-I transport assay, cells were fixed with 4% PFA/PBS(−) and then treated as above except for the use of 1% BSA/PBS(−) instead of 0.1% gelatin/PBS(−).

Mander's coefficient correlation between GFP-MISSL and mCh-ALG-2 was calculated by ImageJ JACoP plugin using threshold values determined manually, and represented as the ratio of GFP-MISSL signals overlapped with mCh-ALG-2 signals to total GFP-MISSL-positive signals. The same threshold values were applied to individual cells before and after amino acid stimulation. Mander's coefficient correlation between Sec31A and ALG-2 was calculated using ImageJ colocalization threshold plugin and represented as the ratio of ALG-2 signals overlapped with Sec31A signals to total Sec31A-positive signals.

Quantification of ERES distribution was done as described previously (16) with minor modifications. In brief, cells were immunostained with Sec16A and γ-tubulin to detect the ERES and the centrosome, respectively, and z-stacks of optical sections spanning the entire cell were captured. Each z-stack was projected onto a single plane, and the cells with a single centrosome adjacent to the nucleus were selected for quantification. The distance of each Sec16A dot excluding nuclear regions from the centrosome was measured using ImageJ. Individual distances in 14 selected cells from two independent siRNA-treated samples were measured.

Mander's coefficient correlation between GM130 and procollagen-I was calculated using ImageJ colocalization threshold plugin. The z-stacks of optical sections were analyzed. Areas of signals derived from procollagen-I were surrounded as regions of interest, and the ratio of procollagen-I signals overlapped with GM130 signals to total collagen type I-positive signals was calculated using automatic threshold values of colocalization threshold plugin. Statistical analysis was done by one-way analysis of variance (ANOVA) followed by Tukey's test.

Quantitative reverse transcription-polymerase chain reaction (RT-qPCR)

Total RNA was isolated from HeLa cells using Sepasol Super G (Nacalai Tesque, Kyoto, Japan), followed by treatment with DNase I (Nippon Gene, Tokyo, Japan). cDNAs were synthesized using a PrimeScript RT reagent kit (Perfect Real Time, Takara), and then qPCR was carried out in LightCycler Nano (Roche Applied Science, Penzberg, Germany) using FastStart Essential DNA Green Master (Roche Applied Science) and primers for spliced XBP1 (5′-CTGAGTCCGAATCAGGTGCAG-3′ and 5′-ATCCATGGGGAGATGTTCTGG-3′) and for total XBP1 (5′-TGGCCGGGTCTGCTGAGTCCG-3′ and 5′-ATCCATGGGGAGATGTTCTGG-3′) according to the manufacturer's instructions.

Mass spectrometry

HeLa cells stably expressing EGFP or EGFP-MISSL grown on four 100-mm dishes were washed once with ice-cold PBS and lysed with lysis buffer A. After centrifugation at 9,000 × *g* for 10 min, the supernatant was pre-cleared by incubating beads (bab-20, Chromotek) for 3.5 h. The pre-cleared lysates were then incubated with GFP-trapA for 3 h, and the beads were washed three times with buffer A. The proteins were resolved by SDS-PAGE, followed by silver staining. The bands were excised and digested with trypsin (Promega, Madison, WI). The resulting peptides were analyzed by Triple TOF 5600+ (AB Sciex, Framingham, MA) essentially as described previously (24).

SEAP assay

HeLa cells stably expressing SEAP seeded in 12-well plates were transfected with siRNAs. After 48 h, the cells were washed once with the medium and then incubated in 600 μl of a fresh medium for 60 min. For the BFA addition experiment, BFA was included in the fresh medium at the final concentration of 2 μg/ml. An aliquot of the medium was centrifuged at 500 × *g* for 1 min, and the medium was analyzed to measure secreted SEAP activity using the Phospha-Light system (Applied Biosystems, CA) and the luminometer (ATTO AB-2250, Tokyo, Japan). For measuring cellular SEAP activity, cells were washed twice with PBS(−) and then lysed with a buffer containing 0.2% Triton X-100 by incubating for 10 min. After centrifugation at 9,000 × *g* for 2 min, cell lysates were analyzed according to manufacturer's instructions. Statistical analysis was done by one-way analysis of variance (ANOVA) followed by Tukey's test.

Procollagen transport assay

Human lung fibroblast IMR-90 cells were transfected with siRNAs. After 48 h, cells were incubated at 40 °C for 3 h. Then the cells were transferred into medium containing 50 μg/ml cycloheximide and 50 μg/ml ascorbate (L-ascorbic acid phosphate magnesium salt *n*-hydrate, Wako), which was prewarmed at 32 °C, and were incubated for 15 min at 32 °C. Immunostaining was done as described under "Indirect immunofluorescence" using the anti-procollagen type I C-peptide antibody and the anti-GM130 rabbit polyclonal antibody. Statistical analysis was done by one-way ANOVA followed by Tukey's test.

Author contributions—T. T. designed and performed the study and wrote the paper. K. I. and Y. A. performed the experiments. K. K. performed the MS analysis. H. S. and M. M. provided advice for the experiment and data analysis and wrote the paper. All authors reviewed the results and approved the final version of the manuscript.

Acknowledgments—We thank Dr. Sasaki-Osugi and all members of the laboratory of Molecular Cell Regulation for their valuable support and discussion. We also thank Dr. Ayano Satoh for providing HeLa cells stably expressing SEAP. The Institute of Transformative Bio-Molecules is supported by the World Premier International Research Center Initiative, Japan.

References

1. Berridge, M. J., Bootman, M. D., and Roderick, H. L. (2003) Calcium signalling: dynamics, homeostasis and remodelling. *Nat. Rev. Mol. Cell Biol.* **4,** 517–529
2. Clapham, D. E. (2007) Calcium signaling. *Cell* **131,** 1047–1058
3. D'Arcangelo, J. G., Stahmer, K. R., and Miller, E. A. (2013) Vesicle-mediated export from the ER: COPII coat function and regulation. *Biochim. Biophys. Acta* **1833,** 2464–2472
4. Brandizzi, F., and Barlowe, C. (2013) Organization of the ER-Golgi interface for membrane traffic control. *Nat. Rev. Mol. Cell Biol.* **14,** 382–392
5. Chen, J.-L., Ahluwalia, J. P., and Stamnes, M. (2002) Selective effects of calcium chelators on anterograde and retrograde protein transport in the cell. *J. Biol. Chem.* **277,** 35682–35687
6. Hay, J. C. (2007) Calcium: a fundamental regulator of intracellular membrane fusion? *EMBO Rep.* **8,** 236–240
7. Helm, J. R., Bentley, M., Thorsen, K. D., Wang, T., Foltz, L., Oorschot, V., Klumperman, J., and Hay, J. C. (2014) Apoptosis-linked gene-2 (ALG-2)/Sec31 interactions regulate endoplasmic reticulum (ER)-to-Golgi transport: a potential effector pathway for luminal calcium. *J. Biol. Chem.* **289,** 23609–23628
8. Maki, M., Kitaura, Y., Satoh, H., Ohkouchi, S., and Shibata, H. (2002) Structures, functions and molecular evolution of the penta-EF-hand Ca^{2+}-binding proteins. *Biochim. Biophys. Acta* **1600,** 51–60
9. Suzuki, H., Kawasaki, M., Inuzuka, T., Okumura, M., Kakiuchi, T., Shibata, H., Wakatsuki, S., and Maki, M. (2008) Structural basis for Ca^{2+}-dependent formation of ALG-2/Alix peptide complex: Ca^{2+}/EF3-driven arginine switch mechanism. *Structure* **16,** 1562–1573
10. Missotten, M., Nichols, A., Rieger, K., and Sadoul, R. (1999) Alix, a novel mouse protein undergoing calcium-dependent interaction with the apoptosis-linked-gene 2 (ALG-2) protein. *Cell Death Differ.* **6,** 124–129
11. Vito, P., Pellegrini, L., Guiet, C., and D'Adamio, L. (1999) Cloning of AIP1, a novel protein that associates with the apoptosis-linked gene ALG-2 in a Ca^{2+}-dependent reaction. *J. Biol. Chem.* **274,** 1533–1540
12. Yamasaki, A., Tani, K., Yamamoto, A., Kitamura, N., and Komada, M. (2006) The Ca^{2+}-binding protein ALG-2 is recruited to endoplasmic reticulum exit sites by Sec31A and stabilizes the localization of Sec31A. *Mol. Biol. Cell* **17,** 4876–4887
13. Shibata, H., Suzuki, H., Yoshida, H., and Maki, M. (2007) ALG-2 directly binds Sec31A and localizes at endoplasmic reticulum exit sites in a Ca^{2+}-dependent manner. *Biochem. Biophys. Res. Commun.* **353,** 756–763
14. la Cour, J. M., Mollerup, J., and Berchtold, M. W. (2007) ALG-2 oscillates in subcellular localization, unitemporally with calcium oscillations. *Biochem. Biophys. Res. Commun.* **353,** 1063–1067
15. Satoh, H., Shibata, H., Nakano, Y., Kitaura, Y., and Maki, M. (2002) ALG-2 interacts with the amino-terminal domain of annexin XI in a Ca^{2+}-dependent manner. *Biochem. Biophys. Res. Commun.* **291,** 1166–1172
16. Shibata, H., Kanadome, T., Sugiura, H., Yokoyama, T., Yamamuro, M., Moss, S. E., and Maki, M. (2015) A new role for annexin A11 in the early secretory pathway via stabilizing Sec31A protein at the endoplasmic reticulum exit sites (ERES). *J. Biol. Chem.* **290,** 4981–4993
17. Shibata, H., Suzuki, H., Kakiuchi, T., Inuzuka, T., Yoshida, H., Mizuno, T., and Maki, M. (2008) Identification of Alix-type and non-Alix-type ALG-2-binding sites in human phospholipid scramblase 3: differential binding to an alternatively spliced isoform and amino acid-substituted mutants. *J. Biol. Chem.* **283,** 9623–9632
18. Takahashi, T., Kojima, K., Zhang, W., Sasaki, K., Ito, M., Suzuki, H., Kawasaki, M., Wakatsuki, S., Takahara, T., Shibata, H., and Maki, M. (2015) Structural analysis of the complex between penta-EF-hand ALG-2 protein and Sec31A peptide reveals a novel target recognition mechanism of ALG-2. *Int. J. Mol. Sci.* **16,** 3677–3699
19. Maki, M., Takahara, T., and Shibata, H. (2016) Multifaceted roles of ALG-2 in Ca^{2+}-regulated membrane trafficking. *Int. J. Mol. Sci.* **17,** E1401
20. Lo, K. W., Zhang, Q., Li, M., and Zhang, M. (1999) Apoptosis-linked gene product ALG-2 is a new member of the calpain small subunit subfamily of Ca^{2+}-binding proteins. *Biochemistry* **38,** 7498–7508
21. Kitaura, Y., Matsumoto, S., Satoh, H., Hitomi, K., and Maki, M. (2001) Peflin and ALG-2, members of the penta-EF-hand protein family, form a heterodimer that dissociates in a Ca^{2+}-dependent manner. *J. Biol. Chem.* **276,** 14053–14058
22. Katoh, K., Suzuki, H., Terasawa, Y., Mizuno, T., Yasuda, J., Shibata, H., and Maki, M. (2005) The penta-EF-hand protein ALG-2 interacts directly with the ESCRT-I component TSG101, and Ca^{2+}-dependently co-localizes to aberrant endosomes with dominant-negative AAA-ATPase SKD1/Vps4B. *Biochem. J.* **391,** 677–685
23. Okumura, M., Ichioka, F., Kobayashi, R., Suzuki, H., Yoshida, H., Shibata, H., and Maki, M. (2009) Penta-EF-hand protein ALG-2 functions as a Ca^{2+}-dependent adaptor that bridges Alix and TSG101. *Biochem. Biophys. Res. Commun.* **386,** 237–241
24. Kanadome, T., Shibata, H., Kuwata, K., Takahara, T., and Maki, M. (2017) The calcium-binding protein ALG-2 promotes endoplasmic reticulum exit site localization and polymerization of Trk-fused gene (TFG) protein. *FEBS J.* **284,** 56–76
25. Bentley, M., Nycz, D. C., Joglekar, A., Fertschai, I., Malli, R., Graier, W. F., and Hay, J. C. (2010) Vesicular calcium regulates coat retention, fusogenicity, and size of pre-Golgi intermediates. *Mol. Biol. Cell* **21,** 1033–1046
26. la Cour, J. M., Schindler, A. J., Berchtold, M. W., and Schekman, R. (2013) ALG-2 attenuates COPII budding *in vitro* and stabilizes the Sec23/Sec31A complex. *PLoS ONE* **8,** e75309
27. Rayl, M., Truitt, M., Held, A., Sargeant, J., Thorsen, K., and Hay, J. C. (2016) Penta-EF-hand protein peflin is a negative regulator of ER-To-Golgi transport. *PLoS ONE* **11,** e0157227
28. McGourty, C. A., Akopian, D., Walsh, C., Gorur, A., Werner, A., Schekman, R., Bautista, D., and Rape, M. (2016) Regulation of the CUL3 ubiquitin ligase by a calcium-dependent co-adaptor. *Cell* **167,** 525–538
29. Osugi, K., Suzuki, H., Nomura, T., Ariumi, Y., Shibata, H., and Maki, M. (2012) Identification of the P-body component PATL1 as a novel ALG-2-interacting protein by *in silico* and far-Western screening of proline-rich proteins. *J. Biochem.* **151,** 657–666
30. Lefebvre, C., Terret, M. E., Djiane, A., Rassinier, P., Maro, B., and Verlhac, M.-H. (2002) Meiotic spindle stability depends on MAPK-interacting and spindle-stabilizing protein (MISS), a new MAPK substrate. *J. Cell Biol.* **157,** 603–613
31. Zhao, Y., Araki, S., Wu, J., Teramoto, T., Chang, Y.-F., Nakano, M., Abdelfattah, A. S., Fujiwara, M., Ishihara, T., Nagai, T., and Campbell, R. E. (2011) An expanded palette of genetically encoded Ca^{2+} indicators. *Science* **333,** 1888–1891
32. Gulati, P., Gaspers, L. D., Dann, S. G., Joaquin, M., Nobukuni, T., Natt, F., Kozma, S. C., Thomas, A. P., and Thomas, G. (2008) Amino acids activate mTOR complex 1 via Ca^{2+}/CaM signaling to hVps34. *Cell Metab.* **7,** 456–465
33. Maki, M., Suzuki, H., and Shibata, H. (2011) Structure and function of ALG-2, a penta-EF-hand calcium-dependent adaptor protein. *Sci. China Life Sci.* **54,** 770–779
34. Kagan, J. C., Stein, M.-P., Pypaert, M., and Roy, C. R. (2004) *Legionella* subvert the functions of Rab1 and Sec22b to create a replicative organelle. *J. Exp. Med.* **199,** 1201–1211
35. Ong, Y. S., Tang, B. L., Loo, L. S., and Hong, W. (2010) p125A exists as part of the mammalian Sec13/Sec31 COPII subcomplex to facilitate ER-Golgi transport. *J. Cell Biol.* **190,** 331–345
36. Koreishi, M., Yu, S., Oda, M., Honjo, Y., and Satoh, A. (2013) CK2 phosphorylates Sec31 and regulates ER-To-Golgi trafficking. *PLoS ONE* **8,** e54382
37. Amodio, G., Renna, M., Paladino, S., Venturi, C., Tacchetti, C., Moltedo, O., Franceschelli, S., Mallardo, M., Bonatti, S., and Remondelli, P. (2009) Endoplasmic reticulum stress reduces the export from the ER and alters the architecture of post-ER compartments. *Int. J. Biochem. Cell Biol.* **41,** 2511–2521
38. Qin, S.-Y., Kawasaki, N., Hu, D., Tozawa, H., Matsumoto, N., and Yamamoto, K. (2012) Subcellular localization of ERGIC-53 under endoplasmic reticulum stress condition. *Glycobiology* **22,** 1709–1720
39. Amodio, G., Venditti, R., De Matteis, M. A., Moltedo, O., Pignataro, P., and Remondelli, P. (2013) Endoplasmic reticulum stress reduces COPII vesicle formation and modifies Sec23a cycling at ERESs. *FEBS Lett.* **587,** 3261–3266

40. Mizuno, M., and Singer, S. J. (1994) A possible role for stable microtubules in intracellular transport from the endoplasmic reticulum to the Golgi apparatus. *J. Cell Sci.* **107,** 1321–1331
41. Watson, P., Forster, R., Palmer, K. J., Pepperkok, R., and Stephens, D. J. (2005) Coupling of ER exit to microtubules through direct interaction of COPII with dynactin. *Nat. Cell Biol.* **7,** 48–55
42. Caviston, J. P., and Holzbaur, E. L. (2006) Microtubule motors at the intersection of trafficking and transport. *Trends Cell Biol.* **16,** 530–537
43. Villarroel-Campos, D., and Gonzalez-Billault, C. (2014) The MAP1B case: an old MAP that is new again. *Dev Neurobiol.* **74,** 953–971
44. Noble, M., Lewis, S. A., and Cowan, N. J. (1989) The microtubule binding domain of microtubule-associated protein MAP1B contains a repeated sequence motif unrelated to that of MAP2 and tau. *J. Cell Biol.* **109,** 3367–3376
45. Tortosa, E., Galjart, N., Avila, J., and Sayas, C. L. (2013) MAP1B regulates microtubule dynamics by sequestering EB1/3 in the cytosol of developing neuronal cells. *EMBO J.* **32,** 1293–1306
46. Barnat, M., Benassy, M.-N., Vincensini, L., Soares, S., Fassier, C., Propst, F., Andrieux, A., von Boxberg, Y., and Nothias, F. (2016) The GSK3-MAP1B pathway controls neurite branching and microtubule dynamics. *Mol. Cell. Neurosci.* **72,** 9–21
47. Tymanskyj, S. R., Scales, T. M., and Gordon-Weeks, P. R. (2012) MAP1B enhances microtubule assembly rates and axon extension rates in developing neurons. *Mol. Cell. Neurosci.* **49,** 110–119
48. Goold, R. G., Owen, R., and Gordon-Weeks, P. R. (1999) Glycogen synthase kinase 3β phosphorylation of microtubule-associated protein 1B regulates the stability of microtubules in growth cones. *J. Cell Sci.* **112,** 3373–3384
49. Koonce, M. P., and Tikhonenko, I. (2000) Functional elements within the dynein microtubule-binding domain. *Mol. Biol. Cell* **11,** 523–529
50. Jiménez-Mateos, E. M., González-Billault, C., Dawson, H. N., Vitek, M. P., and Avila, J. (2006) Role of MAP1B in axonal retrograde transport of mitochondria. *Biochem. J.* **397,** 53–59
51. Stroissnigg, H., Trancíková, A., Descovich, L., Fuhrmann, J., Kutschera, W., Kostan, J., Meixner, A., Nothias, F., and Propst, F. (2007) *S*-Nitrosylation of microtubule-associated protein 1B mediates nitric-oxide-induced axon retraction. *Nat. Cell Biol.* **9,** 1035–1045
52. Hagiwara, H., Yorifuji, H., Sato-Yoshitake, R., and Hirokawa, N. (1994) Competition between motor molecules (kinesin and cytoplasmic dynein) and fibrous microtubule-associated proteins in binding to microtubules. *J. Biol. Chem.* **269,** 3581–3589
53. Huang, J., Roberts, A. J., Leschziner, A. E., and Reck-Peterson, S. L. (2012) Lis1 acts as a "clutch" between the ATPase and microtubule-binding domains of the dynein motor. *Cell* **150,** 975–986
54. Toropova, K., Zou, S., Roberts, A. J., Redwine, W. B., Goodman, B. S., Reck-Peterson, S. L., and Leschziner, A. E. (2014) Lis1 regulates dynein by sterically blocking its mechanochemical cycle. *Elife* **3,** 10.7554/eLife.03372
55. Jiménez-Mateos, E. M., Wandosell, F., Reiner, O., Avila, J., and González-Billault, C. (2005) Binding of microtubule-associated protein 1B to LIS1 affects the interaction between dynein and LIS1. *Biochem. J.* **389,** 333–341
56. Qin, J., Li, D., Zhou, Y., Xie, S., Du, X., Hao, Z., Liu, R., Liu, X., Liu, M., and Zhou, J. (2017) Apoptosis-linked gene 2 promotes breast cancer growth and metastasis by regulating the cytoskeleton. *Oncotarget* **8,** 2745–2757
57. Qin, J., Yang, Y., Gao, S., Liu, Y., Yu, F., Zhou, Y., Lyu, R., Liu, M., Liu, X., Li, D., and Zhou, J. (2017) Deregulated ALG-2/HEBP2 axis alters microtubule dynamics and mitotic spindle behavior to stimulate cancer development. *J. Cell Physiol.* **232,** 3067–3076
58. Inuzuka, T., Suzuki, H., Kawasaki, M., Shibata, H., Wakatsuki, S., and Maki, M. (2010) Molecular basis for defect in Alix-binding by alternatively spliced isoform of ALG-2 (ALG-2ΔGF122) and structural roles of F122 in target recognition. *BMC Struct. Biol.* **10,** 25
59. Akagi, T., Sasai, K., and Hanafusa, H. (2003) Refractory nature of normal human diploid fibroblasts with respect to oncogene-mediated transformation. *Proc. Natl. Acad. Sci. U.S.A.* **100,** 13567–13572
60. Ran, F. A., Hsu, P. D., Wright, J., Agarwala, V., Scott, D. A., and Zhang, F. (2013) Genome engineering using the CRISPR-Cas9 system. *Nat. Protoc.* **8,** 2281–2308
61. Slaymaker, I. M., Gao, L., Zetsche, B., Scott, D. A., Yan, W. X., and Zhang, F. (2016) Rationally engineered Cas9 nucleases with improved specificity. *Science* **351,** 84–88
62. Sasaki-Osugi, K., Imoto, C., Takahara, T., Shibata, H., and Maki, M. (2013) Nuclear ALG-2 protein interacts with Ca^{2+} homeostasis endoplasmic reticulum protein (CHERP) Ca^{2+}-dependently and participates in regulation of alternative splicing of inositol trisphosphate receptor type 1 (IP3R1) pre-mRNA. *J. Biol. Chem.* **288,** 33361–33375
63. Shibata, H., Inuzuka, T., Yoshida, H., Sugiura, H., Wada, I., and Maki, M. (2010) The ALG-2 binding site in Sec31A influences the retention kinetics of Sec31A at the endoplasmic reticulum exit sites as revealed by live-cell time-lapse imaging. *Biosci. Biotechnol. Biochem.* **74,** 1819–1826
64. Kitamura, T., Koshino, Y., Shibata, F., Oki, T., Nakajima, H., Nosaka, T., and Kumagai, H. (2003) Retrovirus-mediated gene transfer and expression cloning: powerful tools in functional genomics. *Exp. Hematol.* **31,** 1007–1014
65. Takahara, T., Hara, K., Yonezawa, K., Sorimachi, H., and Maeda, T. (2006) Nutrient-dependent multimerization of the mammalian target of rapamycin through the N-terminal HEAT repeat region. *J. Biol. Chem.* **281,** 28605–28614